Flow of warm Atlantic Water in the Norske trough on the East Greenland shelf

Bachelor of Science Thesis

by
Joleen Heiderich

May 18th, 2015

Supervisors:

Dr. Wilken-Jon von Appen[1],
Prof. Dr. Laurenz Thomsen[2],
Prof. Dr. Joachim Vogt[2]

1 Division of Climate Sciences - Physical Oceanography of Polar Seas, Alfred Wegener Institute, Helmholtz Centre for Polar- and Marine Research (AWI), Bremerhaven, Germany
2 Jacobs University Bremen, Bremen, Germany

Abstract

Local water temperature increases associated with global warming have the potential to melt glaciers and ice sheets, which are major contributors to sea level rise. This Bachelor of Science thesis examines the flow of warm (0 °C – 2 °C) Atlantic Water (AW) in the Norske trough on the East Greenland continental shelf using an oceanographic section of CTD and ship-board ADCP (SADCP) data collected in June 2014. The Norske trough connects the open ocean to the marine terminating glacier Nioghalvfjerdsfjorden at 79.5° N and it is of interest whether warm water can flow through this trough to the floating ice tongue.
The CTD data shows that AW with temperatures of 1.5 °C and salinities of 34.5 is overlain by Polar Water (PW) with temperatures of -1.5 °C and salinities of 31.5. The stratification is strong and the halocline is located at a depth of 100 m. The SADCP data was detided using the barotropic tidal model AOTIM5 and it shows that the flow reaches velocities along the trough of up to 0.15 m s^{-1} in the upper 250 m. The absolute geostrophic velocities calculated using the SADCP data, as well as the Rossby radius of 12 - 14 km calculated from the stratification, support the assumption that a bi-directional flow with an in- and outflow exists in the trough. Hence it is shown that warm AW reaches the Norske trough and flows into the direction of the 79.5° N glacier at a depth where it could potentially melt the glacier or its floating ice tongue.
As a precursory step, it was attempted to calibrate lowered ADCP (LADCP) data in order to remove compass deviations that were assumed to be caused by a steel block in the vicinity of the CTD rosette. The data of both the upward and the downward looking LADCP were compared to the SADCP data in order to determine the compass deviation. It was found that in this case this method cannot be used to gain more information about the flow below 250 m depth because the compass deviations vary over time and between stations. It is proposed that this is due to the electromagnetic influence of coiled cables that were located close to the instrument.

Contents

List of Figures

List of Tables

Listings

1 Introduction

1.1 Introduction to the region

The flow along the East Greenland shelf is characterized by two distinct water masses that are both flowing southward in the East Greenland current: cold, fresh Polar Water (PW) emanating from the north, and warm, saline Atlantic Water (AW) originating from the south (Budéus et al., 1997; de Steur et al., 2009). This is schematically shown in a polar stereographic projection map of the Arctic in Figure 1 (Jakobsson et al., 2012). The PW end member is defined as having temperatures below 0 °C and salinities below 34.5 (Bourke et al., 1987). In contrast, AW originally has temperatures exceeding 3 °C and salinities above 34.9 (Bourke et al., 1987). Mixtures of those two end member water masses can be found over the shelf where the properties of both water masses have been significantly altered. The warm AW cools as it flows northward, while the salinity of the relatively fresh PW increases when flowing southward. Salt rejection during sea ice formation can increase the salinity of PW. Generally, the colder PW originating from the Arctic overlies the warmer AW flowing into the region from the east and south from the Atlantic. PW is constrained to the top 200 m (Bourke et al., 1987).

[Figure 1 about here.]

The bathymetry on the East Greenland shelf is poorly surveyed due to it being covered by thick sea ice most of the year (Bourke et al., 1987). In Figure 3 we use the International Bathymetric Chart of the Arctic Ocean (IBCAO) Version 3.0 (Jakobsson et al., 2012). As described in Arndt et al. (2015), an improved interpretation of the bathymetry is based on a reprocessing of all soundings collected in this region (Figure 2). A comparison with this best available compilation reveals that the shallow area in the Norske trough reported by the IBCAO bathymetry is unlikely. Furthermore, an elevation of this size would be expected to influence ocean current velocities because it disturbs the along-isobath flow. This has not been observed to date.

The water on the Northeast Greenland shelf may flow in a clockwise, anticyclonic gyre through a trough system (Bourke et al., 1987), but this is still the topic of active debate. The Norske trough, the Belgica trough and the Westwind trough might form a continuous pathway for AW at depths exceeding 200 m (Bourke et al., 1987). This assumption is supported by the results of water mass tracing experiments conducted by Bignami and Hopkins (1997).

[Figure 2 about here.]

[Figure 3 about here.]

The ice cover on the East Greenland shelf varies seasonally and interannually, which results in a semi-permanent polynya. The so-called Northeast Water (NEW) polynya, an area of open water surrounded by sea ice, is located at approximately 80° N and 15° W (Bourke et al., 1987; Topp and Johnson, 1997). The CTD data evaluated in this project were taken in a another polynya around 77.5° N and 16° W that tends to form in spring/ early summer (Figure 4). Both polynyas are created by winds that blow mobile sea ice further offshore. On the side, closer to the shore, the polynyas are bordered by fast ice. Fast ice does not move with respect to the seafloor because it is frozen to icebergs that are grounded on shallow topography. Those icebergs originate from the Nioghalvfjerdsfjorden glacier at 79.5° N.

[Figure 4 about here.]

The Nioghalvfjerdsfjorden glacier (also known as ”79.5 N glacier”) is a marine terminating glacier with a floating ice tongue extending into the sea. The ice tongue forms an interface of ocean and glacier where oceanic water could potentially melt the ice, depending on its temperature. Melting can only occur above the freezing point, which is 0 °C for freshwater at atmospheric pressure and -0.3 °C at 400 m depth. Due to its salt content, seawater has a lower freezing temperature of e.g. -1.9 °C for a salinity of 35. Figure 5 shows a presumed cross-section of the floating ice tongue of the glacier based on a small amount of measurements (Mayer et al., 2000). This cross-section suggests that the ocean-glacier interface can reach depths of up to 600 m. At those depths, warm AW with temperatures above the freezing point of freshwater might be present and could possibly melt the glacier.

The point where marine terminating glaciers start to float is called the grounding line. The ice that passes this line contributes to increasing sea levels. When the ice that has passed the grounding line melts, the glacier flows faster because the counteracting force that the floating ice tongue exerts is decreasing. A positive feedback mechanism can ensue when the grounding line retreats.

Nevertheless, it has to be remembered that to date no measurements of seawater temperatures exist directly below the floating ice tongue. Therefore it is unknown whether AW actually reaches this location and melts the ice tongue. These circumstances motivated this project and are the reason for several *R/V Polarstern* cruises in the region both in the past and in the future. In this Bachelor Thesis the Norske trough is of special interest because it connects the open ocean to the 79.5 glacier and thus it provides the only entry for the warm AW to the floating ice tongue.

[Figure 5 about here.]

1.2 Compass deviations

Iron in the vicinity of compasses result in compass deviations because compasses point in the direction of the ambient magnetic field. The ambient magnetic field is the sum of both the Earth's magnetic field and the magnetic field of any magnetic materials (like soft and hard iron) or electromagnets close-by. Magnetically hard iron retains the magnetic field that it has been exposed to when it cooled from the liquid phase, whereas soft iron aligns its magnetic dipoles with the ambient magnetic field. This is called magnetic induction. Due to its iron content, steel also displays these two different kinds of magnetic behaviors (von Appen, 2015).

Significant amounts of iron in the vicinity of compass-dependent instruments such as Acoustic Doppler Current Profilers (ADCPs) can induce large errors in the measurements due to incorrect heading recordings. These effect can e.g. also impact measurements from a lowered ADCP (LADCP) on a rosette with a steel weight.

Another source that can influence the heading measurements of such instruments are long, coiled cables that are attached to the rosette. Those coiled cables can develop substantial electromagnetic fields, which can affect compasses in addition to other magnetic materials.

As a second component to this report, the reasons for the compass deviations recorded by the LADCP on *R/V Polarstern* are investigated.

1.3 Motivation

This Bachelor of Science Thesis project aims to answer the following questions:

- What is the flow structure in the Norske trough?
- How can the compass deviations encountered in *R/V Polarstern's* LADCP data be corrected?

The answers to both questions questions are discussed with respect to their implications for the flow towards the glacier. The results support the investigation of whether the warm AW contributes to the melting of the 79.5 N glacier.

Different methods can be used to answer the main question about the potential melting: shipboard measurements and stationary instruments that record time series (such as moorings) can support the investigation, as well as theoretical calculations and model runs. In this case, it was decided to use a combination of different methods. This report uses CTD, LADCP and SADCP measurements that were conducted from *R/V Polarstern*. Furthermore, it investigates mooring data collected in the Westwind trough in 1992/1993. To promote further evaluation of the flow structure on longer time scales in the future, the Alfred Wegener Institute has deployed seven moorings in the Norske trough in June 2014, which have not been recovered yet. Moreover, projects trying to model the flow conditions in the region have been initiated.

2 Data and Instruments

The data used in this project were mainly collected during the *R/V Polarstern* cruise PS85 ARK-XXVIII/2 in June 2014. A detailed cruise report with information on the shipboard setup is Schewe (2015). Here we summarize the most important technical aspects, setups and possible error sources for the instruments used in this Bachelor Thesis project.

2.1 CTD

Profiles of different parameters were obtained using a Sea-Bird Electronics Conductivity Temperature Depth (CTD) sonde (SBE 911+) mounted in a rosette (SBE32) with 22 Niskin bottles for water sampling (Figure 6). The CTD was equipped with dual sensors to record in-situ temperature (SBE3) and conductivity (SBE4). It also contained a Digiquartz 410K-134 pressure sensor. Derived quantities, such as potential temperature θ, potential density σ, in-situ density ρ, salinity, and depth, were calculated from these measurements using standard routines. The CTD measured oxygen concentration with an oxygen sensor (SBE43). It also carried a beam transmissometer (WET Labs C-Star) and a chlorophyll *a* fluorometer (WET Labs ECO-AFL/FL).

The conductivity sensor was calibrated using 41 water samples taken at selected stations. The salt content of those samples was determined using the Optimare Precision Salinometer on-board *R/V Polarstern* by comparing it to standard seawater provided by Ocean Scientific International. Similarly, the oxygen sensor was calibrated using water samples from 12 different stations. The oxygen content in those samples was measured using a titration method.

A steel weight is mounted inside the CTD frame to reduce rotations of the rosette during the CTD casts. It is composed of super duplex stainless steel with a microstrucure of 50:50 austenite and ferrite. Although a steel weight used for this purpose should be non-magnetizable, the material data sheet for the *R/V Polarstern* steel weight states that the material is actually magnetizable (Figure 7). However, the magnetizability may depend on temperature and it has not been definitely clarified yet whether the steel weight is magnetizable or not.

[Figure 6 about here.]

[Figure 7 about here.]

12 CTD stations were taken along the fast ice edge from 77° 23.280’ N 16° 18.300’ W northeastward to about 78° 2.520’ N 14° 2.700’ W, between 14 June 2014 14:00 UTC and 15 June 2014 20:50 UTC (Figure 2, Table 1). Due to ice conditions and mooring

deployments in-between, the CTD casts on the transect were not taken in zonally increasing order and are also not exactly located on a straight line.

2.2 LADCP and SADCP

During the cruise, ocean current velocities were measured using both lowered Acoustic Doppler Current Profilers (LADCPs) and a ship-board Acoustic Doppler Current Profiler (SADCP).

LADCP

During all CTD casts, full-depth profiles of current directions and magnitudes were obtained by two LADCPs, one looking upward and the other one facing downward. The 150-kHZ RDI WorkHorse ADCPs were mounted on the rosette at the positions of bottles 21 and 22 and they were set to ping every second. In the upper water column, approximately 100 m vertical sampling were reached using 27 bins of 4 m height each. In greater depth, only a few of the deeper bins recorded valuable data due to lack of sufficient scatterers. To adapt to the LADCP data acquisition speed, the CTD rosette's maximum vertical speed was set to 1 m s^{-1}. The LADCP setting file `master.txt` containing the instrument parameters that were used for the data collection with the downward looking LADCP during the cruise PS85 is shown in Listing 1.

When a preliminary plot of detided ocean current velocities was plotted, it did not show any coherent current structures. It was concluded that the LADCP data needs to be further processed.

PS85 was only the second cruise where the LADCP was used. The instrument had been inaugurated during the *R/V Polarstern* cruise ANT-XXVIII/3 to Antarctica in 2012. The data collected with the LADCP during this cruise showed plausible results and no obvious signs of compass deviations. However, the 2012 data was not investigated intensely because it has not been published yet. During the ANT-XXVIII/3 cruise, the steel weight was already mounted to the CTD rosette. Thus the instrument set-up was comparable for 2012 and 2014.

SADCP

The ocean current velocities in the upper 300 m of the water column were measured using the SADCP on-board *R/V Polarstern*. The 150-kHz RDI Ocean Surveyor instrument was mounted in the keel of the ship and set to a narrowband mode. The ping rate was configured to 3 s and later increased to 1.1 s. The bin size was 4 m, which results in vertical profiling from 15 m to 200 – 300 m depending on sea state, ship speed, ice conditions and backscatter signals.

Especially low backscatter signals and shallow water depths decrease the velocity resolution. Moreover, interferences with other acoustic signals such as the vessel's Doppler log at 79 kHz and particularly the sediment echolot PARASOUND at 18 kHz negatively influence the velocity data. Other acoustic interferences might be caused by the multibeam echosounder HYDROSWEEP at 15.5 kHz and mooring release signals.The multibeam echosounder HYDROSWEEP is a type of sonar that is used to map the ocean floor and to acquire water depth information.

To receive current directions with respect to geographic north and not to the ship track, the vessel's GPS system was used. Only during some short occasions the communication with the GPS was lost. Recording of the data and setting of the SADCP's operating parameters was done using the VmDas software provided by Teledyne RD instruments.

Two configuration changes were carried out in shallow shelf areas: 2 and 3 m bins in broadband mode were applied first, and then a configuration in broadband mode with bottom track pings (one bottom track ping for each water track ping) was tested during a 22 h long section.

A misalignment angle of -44.352° and a velocity scaling factor of 1.033604 were found after standard calibration of the SADCP (Münchow, 2014). For this project, the calibrated SADCP data are assumed to be accurate enough that no further processing has to be done.

2.3 Moorings

The analysis of this project is partially also based on mooring data collected in 1992/ 1993 in the Westwind trough. Moorings are instrumentations that are attached to the sea floor, which record time series of different properties of the water column until they are recovered usually one or two years after their deployment. During the *R/V Polarstern* cruise PS85 ARK-XXVIII/2 in June 2014, further moorings were deployed in the Norske trough. In the future, those should facilitate a better assessment of the flow conditions in the region.

Westwind trough moorings from 1992/1993

To assess the reliability of the barotropic tidal model AOTIM5, data from four current meter moorings in the Westwind trough region of the NEW polynya was considered (Figure 2). This mooring array was deployed in late July and early August 1992 and recovered approximately one year later. It measured current speeds and directions at three standard depths (75 m, 150 m, 250 m). The moorings were located at 80° 30’ N 14° 37’ W (mooring A), 80° 17’ N 13° 45’ W (mooring B), 80° 19’ N 11° 0’ W (mooring C) and 80° 34’ N 11° 4’ W (mooring D). Further details can be found in Topp and Johnson (1997).

Norske trough moorings from 2014/2015

Seven moorings with 75-kHz ADCPs were deployed along the line of the CTD casts from 77° 23.388’ N 16° 17.832’ W to 77° 59.850’ N 14° 18.612’ W on 14 June and 15 June 2014 (Figure 2). Although the moorings were designed by two different institutions (the

University of Delaware (USA) and the Alfred Wegener Institute) and use different setups, all moorings record temperature and salinity near the bottom and velocity throughout the water column. The mooring design of the AWI moorings is shown in Figure 8.

[Figure 8 about here.]

2.4 AOTIM5 model

AOTIM5 is a barotropic inverse tidal model of the Arctic Ocean (Padman and Erofeeva, 2004). The graphical user interface (GUI) of the AOTIM5 model allows the user to extract the tidal constants (eastward velocity amplitude u, northward velocity amplitude v and tidal elevation amplitude z) for the major tides M_2, S_2, N_2, K_2, K_1, O_1, P_1, Q_1 at a selected location (Figure 9).

[Figure 9 about here.]

3 Part I: LADCP calibration attempt

The processing of the LADCP data was not flawless from the beginning: In addition to the detided ocean current velocity plot that did not display any coherent current structures, it was noticed that the headings of the upward and downward looking LADCPs deviated from each other (Figure 10c). The difference of the compass headings between the two instruments as a function of the heading of either the upward looking LADCP or the downward looking LADCP shows a roughly sinusoidal deviation curve (Figures 10a and 10c). The headings measured at every time step by the two LADCPs differ by up to 40°, although they are not expected to deviate if they are aligned in the installation. When the heading deviations were investigated for each station individually, a high time variability in the headings was noticed. The heading deviations between the upward and the downward looking LADCPs differed from station to station and they did not always display a roughly sinusoidal deviation curve (e.g. Figure 11a and 11b).

This compass deviation effect was assumed to be caused by the steel weight in the center of the CTD rosette. The LADCPs measure current speeds and directions with respect to the instrument's direction. The direction of the flow with respect to geographic north can be determined using the instrument's heading recorded by a magnetic compass. However, this compass is not only influenced by Earth's magnetic field, but also by any other magnetic materials in its vicinity, such as the steel weight and possibly also the frame of the rosette or surrounding electromagnets. Accordingly, the headings do not point in the direction in which the instrument was actually pointing and therefore also the infered current directions are incorrect. Although both the upward and the downward looking LADCP are probably influenced by the same sources, deviations in the headings can be explained by different distances of the two instruments to the magnetic source. The lower LADCP compass is located closer to the steel weight and therefore it was assumed that the compass deviations are more pronounced for the downward looking LADCP.

[Figure 10 about here.]

Since the LADCP data cannot be used without further processing and compass corrections, this section aims to answer the question:

- How can the compass deviations encountered in *R/V Polarstern's* LADCP data be corrected?

Initially, it was planned to correct the compass headings using the method described in von Appen (2015) by comparing the LADCP data to the SADCP data. The SADCP measurements are assumed to reflect the ocean current directions correctly. In order to find a pattern for the compass deviations and the errors occurring during the LADCP data processing, all the LADCP stations during the *R/V Polarstern* cruise PS85 were investigated, not only the ones in the Norske trough.

3.1 Methodology

The data analysis in this Bachelor of Science Thesis was performed using MATLAB®. To process the LADCP raw data, the Lowered ADCP processing software *LADCP 2.0.0b* by C. Mertens (University of Bremen) was used. This program implements the procedures shear method (Fischer and Visbeck, 1993) and inverse method (Visbeck, 2002) and provides a graphical user interface, which can be called by typing `ladcp` into the MATLAB® command line.

The file `updown.m` reads the raw data into a structure `l`, which contains all the necessary information needed for the LADCP processing for both the upward and the downward looking LADCP. [1] A list and an explanation of all the different parameters contained in structure `l` is given in Table 2. For more information on how this processing software is implemented and what the different variables mean, please check the files `updown.m`, `soundspeedcorr.m` and `readpar.m`.

The downward looking LADCP is also called the *master* because it pings before the upward looking LADCP in order to avoid acoustic interference. The upward looking LADCP is also referred to as the *slave* because *master* and *slave* are electronically coupled, such that the *slave* has to follow every ping of the *master*. The distance that is needed between two acoustic signals in order to avoid interference is called blank

[1] The discussed data can be found in the file `all_LADCP_data.mat`.

after transmit.

The LADCP processing software processes *master* and *slave* simultaneously. Furthermore, the software also applies a sound speed correction to the velocity data. The LADCP automatically computes the sound speed based on the measured temperature and an assumed salinity and transducer depth. The instrument uses the sound velocity to convert velocity data into engineering units and to compute distances along the beams. Since the velocity scale factor is proportional to the speed of sound measured by the transducer, the sound velocity can be used to correct for erroneous velocities (i.e. if the assumed salinity is wrong). This post-processing step is conducted by the LADCP processing software.

To check whether only one of the LADCP measured incorrect headings, it was also tried to process the upward looking LADCP and the downward looking LADCP independently with the software by changing the `.par` files. Those files contain the processing parameters used by the LADCP processing software (example file: 2). In order to solely process the *master*, the entry `SLADC...` was removed while keeping the second line empty. If the *slave* is supposed to be used, the entry `MLADC...` has to be replaced with the `SLADC...` entry, again keeping the second line empty.
The LADCP processing software is not able to distinguish upward looking and downward looking LADCP, it processes both in the same way as a downward looking LADCP. Thus, no further information was gained.

3.2 Results

3.2.1 Possible errors

During the processing of the LADCP data, different kinds of errors were encountered for different stations. We now describe typical errors that may occur.

In some cases, the raw data vertical velocity for *master* and *slave* were shifted against each other (Figure 11c). This phenomenon often coincided with a bending down of the surface trace in the raw trace echo intensity plot (Figure 11f) and a non-sinusoidal, random scatter plot in the compass deviation plot (Figure 11a, compare to Figure 10). This random scattering shows that there is no correlation between the headings recorded by the upward looking and the downward looking LADCP. This effect is probably caused by errors in the time assignment for different measurements, such that the headings of the uplooking LADCP are not plotted against the headings of the downlooking LADCP that they actually correspond to. Sometimes, the bottom trace in the raw trace echo intensity plot was also very wavy, particularly for station 425-01 (Figure 11e). At station 443-01 there was again a problem with the time assignment for the measurements, which resulted in a depth vs. time plot that is not a function (Figure 11d). This erroneous station is also apparent in the compass deviation plot (Figure 11b, compare to Figure 10). A complete list of all CTD and LADCP stations showing the errors that occurred during the LADCP data processing can be found in Table 3.

[Figure 11 about here.]

To exclude the possibility that the heading deviations in Figure 10 were caused by a displacement between the coordinate systems of upward looking and downward looking LADCP, roll, pitch and the resulting inclination were compared for both instruments. Inlination was calculated as

$$inclination = \arctan \sqrt{\tan^2(roll) + \tan^2(pitch)}. \tag{1}$$

The upward looking and downward looking LADCP always recorded almost the same values for roll and pitch, and therefore it can be concluded that the beam coordinate systems of both instruments were aligned (Figure 12). In contrast to the heading measurements, we know that the roll and pitch measurements are not subject to compasses deviations caused by (electro-)magnetic disturbances in the vicinity of the instrument. Those variables are measured by an accelerometer instead of a compass. An accelerometer is an instrument which measures direction based on gravitational acceleration. Thus an accelerometer is independent of the magnetic field, but a compass is not. Furthermore, the accelerometer measurements almost always stayed below the maximum recordable inclination threshold of 24°, such that we can assume that the accelerometer measured correctly.

Since there was no time offset between the pitch and roll measurements of the upward and the downward looking LADCPs, we can exclude inaccurate time measurements by the LADCP clocks as a potential error source. The time offset recognized at some stations must be related to other factors, possibly some errors in the processing or recording of the LADCP data.

[Figure 12 about here.]

3.2.2 Assignment of SADCP data points to LADCP data points

To calibrate the LADCP data and to be able to remove the compass deviations using the method described in von Appen (2015), LADCP and the SADCP ocean current velocity measurements were compared for the upper water column where the SADCP measured. Accordingly, the LADCP measurements were matched or assigned to one specific SADCP data point that it was closest to in space and time. Since the LADCP only measured at discrete stations and also reaches deeper than the continuously measuring SADCP, certain selection criteria were applied. Specifically, those were used in order to exclude the influence of the errors named above. The Matlab® codes that

were used to carry out those assignments and to select the LADCP and SADCP measurements that pass the selection criteria can be found in Listings 3 and 4.
The SADCP and LADCP data only was matched where the time difference was less than one minute and the distance was less than 10 meter. Assuming that the shear is small, the measurements should be comparable under these conditions. The percent good value for the SADCP had to be higher than 90 %. Percent good reports the amount of pings that passed a manufacturer-defined threshold of data rejection. The error velocity of the LADCP had to be smaller than 0.04 m s^{-1} or 50 %. Error velocity is defined as the difference between the two estimates of vertical velocity. The instrument only needs three beams to compute three-dimensional velocity, such that the redundant fourth beam can be used to evaluate the assumption of horizontal homogeneity and the data quality (Teledyne, R. D. I., 2011). Furthermore, if the ocean current speeds detected by either the LADCP or the SADCP were smaller than 0.04 m s^{-1} or bigger than 0.2 m s^{-1}, then those measurements were excluded. The upper 60 m of the water column where the LADCP compass might be influenced by its vicinity to the steel hull of *R/V Polarstern* were not taken into account for the LADCP data, as well as the last 20 m above the bottom. Additionally, the data collected at the stations 413-01, 424-01, 432-01 and 437-01 was disregarded due to erroneous time assignments for the headings recorded at these stations. The chosen selection criteria are stringent and they should theoretically exclude any possible error source that is not related to compass deviations.

If we assume that the shear is small, we have to make sure that the CTD rosette does not rotate too fast, such that it is meaningful to compare headings that were recorded at vertical distances of 10 m as defined in the selection criteria. If the rosette turns too fast, a mechanical compass like in the LADCP does not adjust its heading fast enough. The turn rate of the rosette was calculated as the difference of two consecutive heading measurements divided by the time that passed between both measurements. The turn rates showed a standard normal distribution with magnitudes of less than $8\ ^\circ\ s^{-1}$ in 95 % of the cases. Hence, the turn rate was rather small and it is valid to compare measurements that are 10 m apart in vertical direction.

The heading measurements that passed the selection criteria were not constant over time for both the upward and the downward looking LADCP (Figure 13). Taking all stations into account, all heading directions were covered during the *R/V Polarstern* cruise PS85, although some heading directions are more common. Therefore we know that the magnetic influences in the surroundings of the LADCP were not strong enough to lead to constant compass deviations where the compass always points into the same direction.

[Figure 13 about here.]

3.2.3 Comparison of LADCP and SADCP data

When comparing the current speed measured by the upward looking LADCP to the current speed measured by the SADCP using bivariate histograms, it becomes apparent that the data scatter differs from the idealized expected situation that both instruments measured the same speeds (Figure 14a). The differences are even more pronounced for the comparison between the current directions of SADCP and upward looking LADCP (Figure 14b). Assuming that the SADCP and LADCP should measure the same quantities and that the SADCP is measuring correctly, the correct heading of the LADCP can be calculated as the ocean current direction measured by the SADCP minus the ocean current direction measured by the LADCP plus the uncorrected heading of the LADCP (von Appen, 2015). Using the corrected heading, the deviation between the current directions measured by the SADCP and the upward looking LADCP should be zero, but this is not the case (Figure 14c). Additionally, the corrected upward looking LADCP heading still differs markedly from the heading that was actually measured (Figure 14d). The current and heading measurements conducted with the downward looking LADCP display a comparable pattern (Figure 15). Since both instruments display the same behavior, we know that both the upward and the downward looking LADCP measure the headings and thus the current direction incorrectly. In contrast to previous assumptions, there is no evidence that one of the instruments is affected more strongly. Based on these observations, we cannot determine a sinusoidal compass deviation and the method described in von Appen (2015) can unfortunately and unexpectedly not be used to remove the compass deviations. Calibration of the LADCP data is not possible because the compass deviation appears to be changing over time and from station to station. This becomes obvious when the bivariate histograms data scatters are investigated individually for all stations. There are many strong outliers that deviate from the sinusoidal deviation in each case. Therefore, the LADCP data cannot be used in the following to get more information about the flow towards the 79.5 N glacier. The assumption that the incorrect heading measurements were caused by compass deviations due to magnetic fields in the vicinity of the LADCP is supported by the observation that the measured current directions differ much more strongly from the expected data scatter than the current speeds. Although the current directions only roughly follow the idealized situation, we can assume that the LADCP itself is measuring correctly. Instead, the error must have occurred during the transformation of the velocities from instrument coordinates to Earth coordinates using the compass. The surface cutoff in the selection criteria was set to 60 m because it was speculated that the steel hull of *R/V Polarstern* influences the LADCP current velocity measurements. If the is set to 20 m instead, more data points pass the selection criteria, but no qualitative change is observed in the data scatter. Accordingly we conclude that the magnetic steel hull of the ship is not the main factor influencing the compass of the LADCP.

[Figure 14 about here.]

[Figure 15 about here.]

3.3 Discussion

3.3.1 Potential error sources

The high time variability of the compass deviations cannot be explained with permanent or induced magnetism with similar amplitudes as in von Appen (2015). Although the steel weight and other magnetic materials in the vicinity of the instrument might also have an influence on the compass, they cannot be the main source. Sometimes the recorded headings were almost constant, a fact which can only be explained by very strong magnetic fields in the instrument. Therefore we propose that the deviations are mainly due to another magnetic source than previously expected. We assume that the following scenario explains what happened. During PS85, the long cables of the LADCP were coiled up and fixed close to it. These cables might have caused compass deviations when it acted as an electromagnet. Since the position of the cables was changed almost every station (e..g. when CTD sensors or the set-up had to be changed etc.), this would explain the strong compass variations between the individual stations. Furthermore, the magnetic field created by such a solenoid varies depending on the current, and the current varies depending on the instrument's power consumption. The power consumption again depends on the tasks that the instruments has to perform, so it varies with time. In total, that makes the magnetic field created by such electromagnets highly variable. This scenario also explains why the compass deviations were not noticeable during the cruise ANT-XXVIII/3. Different, shorter cables were used for the LADCP in 2012, such that the cables were less coiled. Additionally, the cables were also fixed further away from the instrument. We assume that the magnetic fields created by coiled cables were very low in comparison to the Earth's magnetic field, unlike in 2014. Additionally, the ANT-XXVIII/3 cruise was investigating the region at approximately 50° S, whereas the PS 85 cruise was concentrating on the region at 78° N. At higher latitudes, the vertical component of the Earth's magnetic field dominates, which impedes compass measurements generally. When the electromagnetic fields formed by coiled cables are stronger than the horizontal magnetic field components, the compass will deviate strongly from magnetic north.

A example calculation shows that magnetic field strength of a solenoid created by the coiled LADCP cable can reach magnitudes that are comparable to the Earth's magnetic field at 78° N.

The magnetic field inside a solenoid is described by the following equation:

$$B(z) = \frac{\mu_0 \mu_r N I}{l}. \tag{2}$$

Here B is the magnetic field, μ_0 is permeability of free space ($1.2566 \cdot 10^{-6}$ H/m), μ_r is the relative permeability, N is the number of turns of the solenoid, I is the current (in A) and l is the length of the solenoid (in m). However, this simple equation cannot be used in our case because the compass was located outside the solenoid.

The magnetic field outside a solenoid is weaker than inside due to cancellation effects of opposing fields from neighboring cells. For a solenoid which is long in comparison to its diameter, the outside magnetic field is close to zero. In our case this condition is not fulfille, the solenoid has only a few windings and the diameter of the solenoid is larger than its length. Therefore we can expect a relatively strong field even outside the solenoid. To find an exact expression for the magnetic field outside of a solenoid, the Biot-Savart law can be used:

$$dB = \frac{\mu_0}{4\pi}\frac{Id\overrightarrow{S} \times \overrightarrow{r}}{\overrightarrow{r}^3}. \tag{3}$$

Due to symmetry and current loops that cancel each other, all the components of the field except for the z-component cancel along the z-axis. The z-axis is defined as the longitudinal axis of the solenoid. Consequently, the magnetic field B at position z for a single current loop ($N = 1$) can be found by integrating the Bio-Savart law, which results in the equation:

$$B(z) = \frac{\mu_0}{4\pi}\frac{Ir^2}{2(r^2 + z^2)^{\frac{3}{2}}}. \tag{4}$$

r is the radius of the loop.

It is more difficult to describe the magnetic field at positions that are not located on the z-axis, because there are no cancellation effects during non-symmetric conditions. As described in Jackson (1975), the exact solutions for magnetic field of a single loop (N 0= 1) in the xy-plane centered at the origin are:

On-axis component:

$$B_z = \frac{\mu_0 I}{2\pi}\frac{1}{\sqrt{(a+r)^2 + z^2}}\left[E(k)\frac{a^2 - r^2 - z^2}{(a-r)^2 + z^2} + K(k)\right] \tag{5}$$

Cylindrical polar radial component:

$$B_\rho = \frac{\mu_0 I}{2\pi}\frac{\frac{z}{\sqrt{r^2 - z^2}}}{\sqrt{(a+r)^2 + z^2}}\left[E(k)\frac{a^2 + r^2 + z^2}{(a-r)^2 + z^2} - K(k)\right]. \tag{6}$$

Here a is the loop radius and $E(k)$, $K(k)$ are complete elliptic integrals of the first and second kind with

$$k = \sqrt{\frac{4ar}{(a+r)^2 + z^2}}. \tag{7}$$

In our case, it is sufficient to compute the magnetic field B along the z-axis. So based on Equation 4, the following equation was used for our example calculations:

$$B(z) = \frac{\mu_0 \mu_r I N}{2L} \left[\frac{x_2}{\sqrt{{x_2}^2 + r^2}} - \frac{x_1}{\sqrt{{x_1}^2 + r^2}} \right]. \tag{8}$$

x_1 is the distance between one end of the solenoid to the magnetic field measurement point at the z-axis and x_2 is the distance between the other end of the solenoid to the magnetic field measurement point. Hence, it is sufficient to specify the shorter distance x_1 and the length l of the solenoid, since $x_2 = x_1 + l$. Knowing that $\mu_{r,water} = 0.999992$, we can assume that the relative permeability of seawater $\mu_{r,seawater}$ is approximately one. We use the following conditions for the example calculations of the LADCP set-up on PS85: The coiled cable solenoid had 5 turns, a length of 0.02 m and a length of 0.1 m (Table 4).

[Table 1 about here.]

A 300-kHz Teledyne RDI Instruments Workhorse Sentinel ADCP has a battery capacity of 450 Wh, a DC input and runs with 20-50 V. It has a power usage of 73.2 Wh/day, so if it pings every second as is common in LADCPs, the battery can last for at least five days. Between pings, the capacitors are recharged. From that we calculate a minimum recharge power of 3.05 W. Assuming a voltage U and a power P of 3.05 W, we can find using that the required current is at least 0.1 A (Equation 9). This current estimation is based on average consumption, it might as well be higher at some instances. This might influence the variability of the compass headings, depending on when the compass instruments take place in comparison to the charging.

$$P = UI \tag{9}$$

The resulting magnetic field $B(z)$ on the z-axis outside of a coiled cable solenoid as calculated from Equation 8 for three different distances x_1 and two different currents I are shown in Table 5.

[Table 2 about here.]

The Earth's magnetic field components in the region of interest (77.5° N 15° W) on 1 June 2014 (Table 6) reached similar magnitudes as the magnetic field strength created by the solenoid in our example calculations. In conclusion, electromagnetic fields created by coiled cables in the vicinity of the LADCP have the potential to influence the compass strongly. The influence depends on the distance between the coiled and the instrument, the number of coiled cables and their position relative to the instrument and to each other. Depending on the alignment of various fields, their can either add up or cancel each other out. Frequent changes of the position and sizes of the solenoids as occurred during PS85 can explain the high variability in the compass deviations.
The assumption that electromagnetic fields created by coiled cables can influence compass headings was confirmed during a short laboratory experiment. A mechanical compass was placed above a solenoid made out of a coiled cable with 5 turns, a radius of 0.07 m and a length of 0.02 m. A direct current of 0.35 mA was applied to the cables. Up to distance of 0.15 m from the solenoid, the compass needle showed influences of the magnetic field created by the coiled cable by moving and changing direction very fast.

[Table 3 about here.]

3.3.2 Possible solutions and suggestions for improvement

In order to avoid compass deviations of the LADCP in the future, the most important factor would be too use shorter cables and to avoid coiled cables as far as possible. If this cannot be avoided completely, the coiled cables should be located as far away as possible from the LADCP compass.

Another method to avoid this problem would be that the compass measurements could be recorded by a gyro compass. The gyro compass has the advantage that it works better at higher latitudes than the usual flux scale compass that is used in the LADCP now and it is also not influenced by magnetic fields. A gyro compass is a type of non-magnetic compass which is based on a fast-spinning disc and rotation of the Earth to automatically find geographical direction. When the headings are recorded in instrument coordinates instead of Earth coordinates, one can calculate the instrument's heading based on compass measurements provided by an outer compass like the gyro compass. If this is possible, it would be great if both the instrument and Earth coordinates could be recorded for comparison. If only one option is available, the instrument coordinates are probably more useful. Hence, the set-up of the LADCP has to be changed because it is currently measuring in Earth coordinates.

It would also be interesting to ask the LADCP producer when the compass measurement takes place in comparison to the charging. This would allow a better estimation of the power consumption and thus of the current during the charging.

It would also be good, if a technician could investigate the LADCP problem further by testing the influence of coiled cables on the LADCP compass with the actual instrument. E.g. it would also be helpful to know whether the steel weight in the CTD rosette of *R/V Polarstern* is magnetizable or not and one could search for other magnetic materials that are mounted onto the CTD rosette. Unfortunately, due to the absence and reparation of *R/V Polarstern* and its LADCP this could not be done in this Bachelor Thesis project. One further additional factor that could be investigated in the future is the influence of setting other parameters in the `.par` files for the LADCP processing software (compare Section 3.2.2 and Listing 4).

4 Part II: Interpretation of an oceanographic section

4.1 Methodology

- **W**hat is the flow structure in the Norske trough?

In order to answer this research question and to get more information about the flow structure of warm AW towards the Nioghalvfjerdsfjorden at 79.5° N and its potential melting, the CTD, SADCP and multibeam echosounde HYDROSWEEP data were projected onto a straight line. The CTD data was gridded and interpolated and the SADCP data was detided and rotated. To check whether the tidal model AOTIM5 model can be used to detide the SADCP data in this region, the tidal components predicted by the model were compared to the tides measured by the moorings in the Westwind trough.

4.1.1 Tidal component analysis for 1992/ 1993 Westwind trough moorings

As a first step, a tidal component analysis was performed for the ocean velocity measurements of the Westwind trough moorings from 1992/1993. Using the MATLAB® toolbox *t_tide* developed by Pawlowicz et al. (2002), a harmonic analysis was applied to all the time series measured by the current meters from moorings A, B, C and D (see Figure 2 for their location). Each mooring was equipped with three current meters at different depths. For mooring D, the upper current meter was broken and thus only two time series were retrieved at this location. First, the major tides were identified for each time series by selecting those tides that together account for 90% of the variance of the major axis.

t_tide uses a least squares fit to the period to estimate the influence of different tides on a time series. In measurements with approximately a one year duration, as used here, annual and semi-annual tides can appear to be pronounced although they are not. Instead, this effect is caused by the seasonal forcing in the signal and therefore annual and semi-annual tides like SA and SSA had to be disregarded in this case.

After excluding annual and semi-annual tides from the major tides identified before, the semi-diurnal tides M_2 and S_2 were found to be the most dominant ones in all the time series. M_2 is the principal lunar tide with a period of 12.42 hours, and S_2 is the principal solar tide with a period of 12.00 hours.

The velocity vectors of the flow caused by the M_2 and S_2 tides resulting from the harmonic tidal analysis for the current meters were compared to the tidal predictions for M_2 and S_2 at each location (Figure 16). Those predictions are based on the AOTIM5 model. The mean from the current meters of each mooring should roughly correspond to the barotropic tide.

In the Westwind trough, both the M_2 and the S_2 tides flow northeastward at all four mooring locations, with the M_2 flow being stronger than the S_2 flow. Except for mooring D, the measurements are in good agreement with the model. The deviations of model and measurements of the S_2 tide for moorings C and D could be further investigated in the future.

Even though the 1992/1993 moorings were located in the Westwind trough, approximately 330 km to the north of the PS85 section, we conclude that the model can be used to detide the ADCP data from the Polarstern Cruise PS85 in June 2014. Nonetheless, the model might not work as well for the new region of interest.

[Figure 16 about here.]

4.1.2 CTD, echosounder and SADCP data projection

The CTD stations were orthogonally projected onto a straight transect (Figure 3). The projection line runs through station 417-1 and station 424-1 and has its origin at 77° 19.908' N 16° 20.418' W. This point is defined as zero section distance. The transect runs from south-west to north-east and forms an angle of 32.95° to north. In order to interpolate the CTD data obtained during the casts in the Norske trough, the MATLAB® toolbox *ppzgrid* was used that grids the data with continuous curvature splines under tension (Smith and Wessel, 1990). This routine fits a cubic function through three data points to achieve a maximally smooth function while excluding extrema that lie outside the data range. The routine was used to grid the individual variables onto a grid with horizontal spacing of 2.5 km and a vertical spacing of 5 m.

In order to determine the along-section bathymetry (used in Figures 17 – 21 and 25 – 27), the bottom depth recorded by the multibeam echosounder HYDROSWEEP was averaged over 200 m including all three crossings of the trough.

The SADCP data was detided using the AOTIM5 model by subtracting the tidal prediction for the different locations from the SADCP data to receive the residual signal that does not depend on tides. Then the SADCP data was projected onto the same straight line as the CTD data. Furthermore, the coordinate system was rotated, such that the x_r-axis with velocity u_r describes the along-section velocity and the y_r-axis with velocity v_r represents the cross-section velocity. Only the data collected between

14 June 2014 01:00 UTC and 15 June 2014 04:15 UTC (Figure 3) was considered in order to exclude a questionable strong along-section flow signal in the middle part of the trough. In addition, only the data points above 250 m depth that fulfilled a percent-good criterion of 70 % were taken into account. For the transect, the velocities of all crossings were averaged over a section distance of 2.5 km. The depth intervals correspond to the individual SADCP processing bins.

4.2 Results and discussion

4.2.1 CTD data

The gridded CTD measurements of potential temperature θ, salinity, oxygen and chlorophyll *a* concentration in the Norske trough were examined (Figure 17 – 20). Warm, saline waters below 100 m depth are overlain by colder and fresher waters, as expected due to the influence of AW and PW. Observed temperatures range from -1.5 to 1.5 °C (Figure 17) and salinities from 31.5 to 34.5 (Figure 18). As is typical in the Arctic, the isopycnals follow the salinity contours because the density equivalent salinity variations are much stronger than the density equivalent temperature variations. Hence, at low temperatures density variations are mostly due to salinity variations. Under these conditions, changes in 1 °C are approximately compensated by salinity changes of 0.1, so the influence of temperature and salinity on density differs by one order of magnitude in the section in the Norske trough. Potential density σ ranges from 25 to 28 kg m^{-3}.

The AW-influenced waters below 200 m have the lowest oxygen content, so they are the least ventilated and have taken the longest time since their last contact with the atmosphere (Figure 19).

The chlorophyll *a* content in the Norske trough was so low at the time of measurement that the instrument had problems to detect it (Schewe, 2015). It often recorded negative chlorophyll *a* concentrations at greater depth, such that only the upper 50 m could be used for the analysis. The chlorophyll *a* sensor was used throughout the cruise and it showed plausible results except for this transect. Larger chlorophyll *a* concentrations were in particular encoutered in the open waters of the eastern Fram Strait. Hence, it was concluded that the instrument measured correctly and that the concentrations were smaller than the measurement range allowed us to detect. Maximum chlorophyll *a* concentrations of up to 2.5 mg m^{-3} were found in the shallower area at the southernmost part of the transect (Figure 20). Chlorophyll *a* is a measure for biological productivity in the ocean. Productivity might have been very low in June 2014 because nutrient depletion following the spring bloom might have prevented further plankton growth or because the macro-nutrient levels on the shelf are very low (Metfies et al., 2015).

Transmissivity, a measure for light transmission, was at a relatively constant high level of 98 % m^{-1} throughout the transect. Only in the southern surface waters in the shallower part of the trough, where oxygen and chlorophyll *a* concentrations were highest, it decreases to up to 88 % m^{-1} possibly due to some biological activity there (not shown). Otherwise, the waters of the section were very clear (compare Figure 4) and in particular no sediments were in the water column.

[Figure 17 about here.]

[Figure 18 about here.]

[Figure 19 about here.]

[Figure 20 about here.]

Bouyancy frequency squared N^2

The buoyancy frequency squared N^2, a measure of stratification, was calculated from the potential density grid using the following equation:

$$N^2 = -\frac{g}{\rho_0}\frac{d\rho}{dz}, \tag{10}$$

where g is the gravitational acceleration (9.81 m s^{-2}), ρ_0 is the average density (here taken as 1025 kg m^{-3}) and ρ is potential density. To assure that density is monotonically increasing with depth and to exclude small fluctuations caused by ship movement and waves, the density grid had to be sorted. The gridded transect of buoyancy frequency squared N^2 highlights the halocline between PW and AW underneath at 100 m depth (Figure 21). It also shows that the old AW waters (Figure 19) in the bottom of the trough below 300 m depth are very weakly stratified. This might be due to the sills in the Norske trough and the fact that water at these depths cannot flow into the trough system below the sill level.

[Figure 21 about here.]

Water masses

Figure 22 and 23 show the different CTD stations in θ-S space. At all stations, very low potential temperature θ close to the freezing line was encountered. The temperature and salinity maxima associated with the core of AW are located in the middle part of the transect where the trough is deepest (Figure 23). This water also has the largest heat capacity and therefore melting potential if it could reach the ice tongue of the 79.5 N glacier.

[Figure 22 about here.]

[Figure 23 about here.]

Rossby radius

The Rossby radius can be calculated from the stratification (Zhao et al., 2014):

$$Ro = \frac{1}{\pi \cdot f} \int_{-H}^{0} N(z')dz'. \tag{11}$$

Here $f = 2\Omega \cdot sin(\phi)$ is the Coriolis parameter, H is the height of the water column, N is the buoyancy frequency, Ω is the rotation rate of the Earth ($7.2921 \cdot 10^{-5}$ rad s^{-1}) and ϕ is the latitude (78° in this case). The Rossby radius along the Norske trough transect is shown in Figure 24. For most of the deep part of the trough (section distances from 10 km to 85 km), the Rossby radius is approximately 12 – 14 km. The majority of the contribution to this stems from the halocline and and the weak stratification at depth only has a minor contribution, which is why the Rossby radius changes much less than the water depth along the section. Around 80 km section distance, the Rossby radius reaches a maximum of 14 km. The Norske trough at this location has a width of more than 80 km, i.e. more than five times the Rossby radius. The width of a geostrophic flow along a sloping side wall scales like the Rossby radius. Hence the Norske trough would support two boundary layers and it is feasible that a bi-directional flow with an in- and an outflow exists.

[Figure 24 about here.]

4.2.2 SADCP data and geostrophic velocity

SADCP data

The along-section velocity u_r as measured by the SADCP reached speeds of up to 0.15 m s^{-1} in both directions (Figure 25). The cross-section velocity v_r reaches the same magnitude (Figure 26). In the upper 250 m, the water at the outer sides of the trough flows towards the open ocean, whereas the flow in the middle part of the trough, as well as in the shallower areas surrounding the trough, is directed towards the 79.5 N glacier.

[Figure 25 about here.]

[Figure 26 about here.]

Geostrophic velocity

Since the LADCP could not be calibrated and the SADCP data only provides information up to a depth of 250 m, the only possibility to get some information about the currents at greater depth is by computing the geostrophic component of the flow. The geostrophic velocity was calculated from thermal wind (Gill, 1982):

$$f\frac{\partial v_r}{\partial z} = -\frac{g}{\rho_0}\frac{\partial \rho}{\partial x_r}. \tag{12}$$

Here v_r is the geostrophic velocity, f is again the Coriolis parameter, g is gravitational acceleration (9.81 m s^{-2}), ρ_0 is the average density (again taken as 1025 kg m^{-3}) and ρ is potential density. Geostrophic velocity describes the cross-sectional flow in which the horizontal pressure gradient force is balanced by the Coriolis force. Since the SADCP grid and the CTD grid coincide after taking the horizontal density gradient, the depth-averaged cross-sectional SADCP velocity v above the pycnocline ($z_{ref} = [30 - 80]$ m) can be used as an integration constant z_{ref} to reference the geostrophic flow calculated from intergrating the shear:

$$v(z - z_{ref}) = -\frac{g}{f \cdot \rho_0}\int_{z'=z_{ref}}^{z}\frac{\partial \rho}{\partial x}dz' \tag{13}$$

$$v(z) = v(z - z_{ref}) + v(z_{ref}) \tag{14}$$

$v(z)$ is then the absolute geostrophic velocity. Similar to the SADCP velocities (Figure 26), the geostrophic flow in the middle part of the trough and in the shallower areas is also directed towards the 79.5 N glacier (Figure 27), while it flows in the opposite direction at the rims of the trough. Maximum absolute geostrophic velocities reach up to 15 m s^{-1} in both directions in the lower parts of the trough. When the averaged SADCP velocity below the pycnocline ($z_{ref} = [130-200]$ m) is used as the integration constant instead, the picture does not change qualitatively.

[Figure 27 about here.]

5 Summary and conclusions

In this Bachelor of Science thesis it was shown that warm AW with temperatures of 1.5 °C and salinities of 34.5 reached the Norske trough on the Northeast Greenland shelf in June 2014. The AW was overlain by Polar Water (PW) with temperatures of -1.5 °C and salinities of 31.5. This two-layer system lead to a strong stratification with the halocline located at a depth of 100 m. If the ocean-glacier interface of the 79.5 N glacier actually reaches depths of up to 600 m, as it is proposed in Mayer et al. (2000), the AW could potentially melt the glacier. The flow in the upper 250 m of the water column reached velocities along the trough of up to 0.15 m s^{-1} in both directions, according to the SADCP data. A bi-directional flow in and out of the trough is also apparent in the absolute geostrophic velocities that were calculated using the SADCP data. The Rossby radius of 12 - 14 km was calculated from the stratification. The Norske trough has a width of more than 80 km at the location of the CTD transect and because the geostrophic flow along a sloping side wall scales like the Rossby radius, this finding also supports the assumption that an in- and outflow exists in the trough. In conclusion, the information that warm AW extents into the Norske trough and reaches a location around 78° N 16° W has been gained. Furthermore it was shown that the AW flows into the direction of the 79.5° N glacier at a depth where it could potentially melt the glacier's floating ice tongue. However, it is still unclear whether the AW extends far enough to the north in the Norske trough to actually reach the glacier. Further investigations using different instruments and models are needed to answer the question whether the floating ice-tongue of the 79.5 N glacier is melting or not. This insight will be very important for the assessment of sea level rise in the future. The Norske trough moorings that will be recovered in 2016 will hopefully provide more information about the seasonal variations of the flow in the region and they are the next step in the investigation of the potential of the 79.5 N glacier.

The LADCP data could unfortunately not be used to gain information about the ocean current velocities below 250 depth due to compass deviations that are proposed to be caused by the electromagnetic influence of coiled cables in the vicinity of the instrument. The calibration attempt revealed that the compass deviation changes with time and from station to station for both the upward and the downward looking LADCP. Compass deviations are very pronounced in both instruments. As a result, the calibration method described in von Appen (2015) could not be applied, other than planned previously. It could not be clarified yet whether steel block in the vicinity of the CTD rosette also exerts a magnetic field at the LADCP compass. This question needs to be further investigated, as well as the existence of other magnetic sources at the CTD rosette. However, the coiled cables were found to be the main magnetic source because they are the only explanation why the magnetic field and hence the compass deviations varied so strongly with time. In order to avoid further compass deviation problems with the LADCP, it was suggested that the headings should be measured using a gyro compass and that the velocity data should be recorded in instrument coordinates in the future.

6 Acknowledgments

We kindly acknowledge the captain and crew of the *R/V Polarstern*. The data used in this work was collected under grant number AWI_PS85_03. Discussions with J. Schaffer, V. Strass and O. Strothmann were very helpful. I would like to thank my supervisors at Jacobs University Bremen , Prof. Dr. Laurenz Thomsen and Prof. Dr. J.Vogt at Jacobs University for their support. A particularly big thank you goes to my supervisor at the Alfred Wegener Institue, Dr. Wilken-Jon von Appen, for answering my numerous question, for helping me out of several Matlab and LaTeX crises and for teaching me incredibly much about physical oceanography.

References

Arndt, J. E., W. Jokat, B. Dorschel, R. Mykkelbust, J. A. Dowdeswell, and J. Evans (2015). The northeast Greenland continental shelf – Insights from a new bathymetric compilation. *In prep.*

Bignami, F. and T. Hopkins (1997). The water mass characteristics of the Northeast Water Polynya: Polar Sea data 1992-1993. *Journal of Marine Systems 10*(1 - 4), 139 – 156.

Bourke, R. H., J. L. Newton, R. G. Paquette, and M. D. Tunnicliffe (1987). Circulation and water masses of the East Greenland shelf. *Journal of Geophysical Research: Oceans 92*(C7), 6729–6740.

Budéus, G., W. Schneider, and G. Kattner (1997). Distribution and exchange of water masses in the Northeast Water polynya (Greenland Sea). *Journal of Marine Systems 10*(1 - 4), 123 – 138.

de Steur, L., E. Hansen, R. Gerdes, M. Karcher, E. Fahrbach, and J. Holfort (2009). Freshwater fluxes in the East Greenland Current: A decade of observations. *Geophysical Research Letters 36*(23).

Fischer, J. and M. Visbeck (1993). Deep Velocity Profiling with Self-contained ADCPs. *Journal of Atmospheric and Oceanic Technology 10*(5), 764–773.

Gill, A. E. (1982). *Atmosphere-Ocean Dynamics.* International Geophysics. Elsevier Science. 662 p.

Jackson, J. D. (1975). *Classical Electrodynamics.* Wiley. 848 p.

Jakobsson, M., L. Mayer, B. Coakley, J. A. Dowdeswell, S. Forbes, B. Fridman, H. Hodnesdal, R. Noormets, R. Pedersen, M. Rebesco, et al. (2012). The international bathymetric chart of the Arctic Ocean (IBCAO) version 3.0. *Geophysical Research Letters 39*(12).

Mayer, C., N. Reeh, F. Jung-Rothenhäusler, P. Huybrechts, and H. Oerter (2000). The subglacial cavity and implied dynamics under Nioghalvfjerdsfjorden Glacier, NE-Greenland. *Geophysical Research Letters 27*(15), 2289–2292.

Metfies, K., W.-J. von Appen, A. Nicolaus, E.-M. Nöthig, S. Hendriks, and E. Kilias (2015). Chl a biomass and Biogeography of Arctic Pelagic Pico-Eukaryotes during the Record Sea Ice Minimum 2012. *Limnology and Oceanography submitted*.

Münchow, A. (2014). Calibration of FS Polarstern's vessel-mounted 153 kHz ADCP. *College of Earth, Ocean and Environment, Newark, Delaware, USA*.

Padman, L. and S. Erofeeva (2004). A barotropic inverse tidal model for the Arctic Ocean. *Geophysical Research Letters 31*(2).

Pawlowicz, R., B. Beardsley, and S. Lentz (2002). Classical Tidal Harmonic Analysis Including Error Estimates in MATLAB using t_tide. *Computers and Geosciences 28*, 929–937.

Schewe, I. (2015). The expedition of the research vessel "Polarstern" to the Arctic in 2014 (PS85 ARK-XXVIII/2). *Berichte zur Polar- und Meeresforschung = Reports on polar and marine research, Bremerhaven, Alfred Wegener Institute for Polar and Marine Research.* doi:10.2312/BzPM_0687_2015.

Smith, W. and P. Wessel (1990). Gridding with continuous curvature splines in tension. *Geophysics 55*, 293.

Teledyne, R. D. I. (2011). Acoustic Doppler Current Profiler: Principles of Operation - A Practical Primer. *RD Instruments, Poway, California, USA*.

Topp, R. and M. Johnson (1997). Winter intensification and water mass evolution from yearlong current meters in the Northeast Water Polynya. *Journal of Marine Systems 10*(1 - 4), 157 – 173.

Visbeck, M. (2002). Deep Velocity Profiling Using Lowered Acoustic Doppler Current Profilers: Bottom Track and Inverse Solutions. *Journal of Atmospheric and Oceanic Technology 19*(5), 794–807.

von Appen, W.-J. (2015). Correction of ADCP Compass Errors Resulting from Iron in the Instrument's Vicinity. *Journal of Atmospheric and Oceanic Technology 32*, 591–602.

Zhao, M., M.-L. Timmermans, S. Cole, R. Krishfield, A. Proshutinsky, and J. Toole (2014). Characterizing the eddy field in the Arctic Ocean halocline. *Journal of Geophysical Research: Oceans 119*(12), 8800–8817.

Appendix

Listing 1: Parameter file `master.txt` showing the settings of the downward looking LADCP that were used during the cruise PS85. The file for the downward looking LADCP, `slave.txt`, looks analogous, with only four small changes: `MLADCP` is changed into *SLADCP* in lines 1 and 7, `SM1` is replaced by `SM2` in line 23 and there is an extra entry `ST03002` inserted between the lines 23 and 24.

```
1 $1C:\LADCP\MLADCP.log
2 $B
3 $W62
4 CR1
5 WM15
6 CB411
7 RN MLADCP
8 LZ030,220
9 CF11111
10 EA0
11 EB0
12 ED0
13 ES35
14 EX11111
15 EZ1111101
16 WB0
17 WD111100000
18 WF176
19 WN27
20 WP1
21 WS400
22 WV175
23 SM1
24 SA001
25 SI0
26 SW75
```

```
TE00:00:01.00
TP00:01.00
CK
CS
$D3
$p Disconnect now
$D7
$1
§X
;
;Instrument          = Workhorse Sentinel
;Frequency           = 307200
;Water Profile       = YES
;Bottom Track        = NO
;High Res. Modes     = NO
;High Rate Pinging   = NO
;Shallow Bottom Mode= NO
;Wave Gauge          = NO
;Lowered ADCP        = YES
;Ice Track           = NO
;Surface Track       = NO
;Beam angle          = 20
;Temperature         = 5.00
;Deployment hours    = 24.00
;Battery packs       = 1
;Automatic TP        = YES
;Memory size [MB]    = 2048
;Saved Screen        = 1
;
;Consequences generated by PlanADCP version 2.06:
;First cell range    = 6.17 m
;Last cell range     = 110.17 m
```

```
;Max range          = 103.66 m
;Standard deviation = 3.55 cm/s
;Ensemble size      = 781 bytes
;Storage required   = 64.35 MB (67478400 bytes)
;Power usage        = 73.20 Wh
;Battery usage      = 0.2
;
; WARNINGS AND CAUTIONS:
; WM15 feature has to be installed has to be installed in Workhorse...
    to use selected option.
; Advanced settings have been changed.
```

Listing 2: Example `.par` file for station 411-02. This file contains the processing parameters used by the LADCP processing software (last three lines), as well as information about the cruise name, the station name, time and location and the station files containing the velocity data for *master* and *slave*.

```
MLADC004.000,411-02.cnv
SLADC004.000
Polarstern,PS85
411-02
77,43.060,-15,-28.700
77,43.050,-15,-28.550
2014,06,14,13,46,59
2014,06,14,14,29,10
1,0,0
19.9,30,2.8,0.1
10,10,10
```

Listing 3: Sample code file `assign_SADCP_to_LADCP.m`: It assigns LADCP data points to the SADCP data points that are closest in space and time (compare Section 3.2.2).

```
%---------------------------------------------------------------------
% Program that assigns SADCP data to the corresponding LADCP
% data matrix (of either the uplooking or the downlooking LADCP)
% from the same location, depth and time

% Last modified: 21 January 2015
% Created by: Dr. Wilken-Jon von Appen, Alfred Wegener Institute
% (AWI) & Joleen Heiderich (Jacobs University Bremen)

%---------------------------------------------------------------------
% EXPLANATION OF THE DIFFERENT PARAMETERS AND THEIR DIMENSIONS:

% FROM LADCP DATA:
% ntl - number of times for LADCP
% ndl - number of depth times for LADCP
% tl - times of LADCP, [1 x ntl]
% ul - u-velocity of LADCP, [ndl x ntl]
% vl - v-velocity of LADCP, [ndl x ntl]
% zl - depth of LADCP, [ndl x ntl]
% el - error velocity of LADCP, [ndl x ntl]

% FROM SADCP DATA:
% nts - number of times for SADCP
% nds - number of depth times for SADCP
% ts - times for SADCP, [1 x nts]
% us - u-velocity of SADCP, [nds x nts]
% vs - v-velocity of SADCP, [nds x nts]
% zs - depth of SADCP, [nds x 1]
% pgs - percent good of SADCP, [nds x nts]
```

```

% VARIABLES THAT ARE NEEDED WITHIN THE PROGRAM:
% dt - absolute time difference between SADCP and LADCP data,
%      [nts x ntl] or [nts x length(inds)] in memory restricted
%      case
% dz - absolute depth difference between SADCP and LADCP data,
%      [ndl x ntl x nds] or [ndl x length(inds) x nds] in
%      memory restricted case
% it_S_L_v - preliminary vector for the creation of the matrix
%            it_S_L, [1 x ntl]
% np - length of the pieces of ntl (might vary for the two
%      loops of the program, see below), [1 x 1]
% memory - memory of the computer available to execute the
%          program, chosen such that it equals approximately
%          one fourth of the RAM of the computer;
%          given in bits, [1 x 1]
% handle_to_uplooking_LADCP - logical; 1 if the uplooking LADCP
%                             data is supposed to be loaded,
%                             0 if the downlooking LADCP data
%                             is supposed to be loaded

% VARIABLES THAT ARE CREATED AND STORED IN THE STRUCTURE A:
% us_at_L - SADCP u-velocity at time and depth of LADCP,
%           [ndl x ntl]
% vs_at_L - SADCP v-velocity at time and depth of LADCP,
%           [ndl x ntl]
% pgs_at_L - SADCP percent good at time and depth of LADCP,
%            [ndl x ntl]
% mt_S_L - minimum time between SADCP and LADCP for the minimum
%          value, [ndl x ntl]
% md_S_L - minimum depth between SADCP and LADCP for the minimum
%          value, [ndl x ntl]
```

```
% it_S_L - index that points from a SADCP entry (us/vs) to the
%           location in the us_at_L/ vs_at_L matrix where it
%           should be stored (time dimension, 2nd dimension in
%           Matlab), [ndl x ntl], the entries in it_S_L can range
%           from 1 to nts and can be repeated
% id_S_L - index that points from a SADCP entry (us/vs) to the
%           location in the us_at_L/ vs_at_L matrix where it
%           should be stored (depth dimension, 1st dimension in
%           Matlab), [ndl x ntl], the entries in id_S_L can range
%           from 1 to nds and can be repeated

%-----------------------------------------------------------------
% LOADING OF THE SADCP AND LADCP DATA AND SETTING OF THE
% PARAMETERS NEEDED:

LADCP = 'D:\Meine Dokumente\Jacobs University Bremen\Bachelor ...
    Thesis\Matlab\Data\LADCP\LADCP_processing\processing\...
    L_one_vector.mat';
% The LADCP data has to be stored in a structure Lv with two
% substructures: Lv(1): upward looking LADCP,
% Lv(2): downward looking LADCP

SADCP = 'D:\Meine Dokumente\Jacobs University Bremen\Bachelor ...
    Thesis\Matlab\Data\SADCP\SADCP_19_35.mat';

SADCP_pg = 'D:\Meine Dokumente\Jacobs University Bremen\Bachelor ...
    Thesis\Matlab\Data\SADCP\PS85_19_35_hc.mat';
% file containing the percent good data of the SADCP

load(LADCP)
load(SADCP)
load(SADCP_pg)
```

```

% select a directory where you want to save the structure A:
filedir = 'D:\Meine Dokumente\Jacobs University Bremen\Bachelor ...
    Thesis\Matlab\Data\SADCP\';

memory = 1e9; % 1GB
handle_to_uplooking_LADCP = 1;

if handle_to_uplooking_LADCP
    ntl = length(Lv(1).time);
    ndl = size(Lv(1).z,1);
    tl = Lv(1).time;
    ul = Lv(1).u;
    vl = Lv(1).v;
    zl = Lv(1).z;
    el = Lv(1).e;
    filename = 'SADCP_assigned_to_LADCP_ul.mat';
    % name structure A uplooking LADCP
else
    ntl = length(Lv(2).time);
    ndl = size(Lv(2).z,1);
    tl = Lv(2).time;
    ul = Lv(2).u;
    vl = Lv(2).v;
    zl = Lv(2).z;
    el = Lv(2).e;
    filename = 'SADCP_assigned_to_LADCP_dl.mat';
    % name structure A downlooking LADCP
end % for handle_to_uplooking_LADCP

nts = length(S.time);
nds = length(S.depth);
```

```
ts = S.time;
us = S.u;
vs = S.v;
zs = S.depth;
pgs = c.pg;

%------------------------------------------------------------------
% EASY PROGRAM VERSION IF THERE IS NO MEMORY RESTRICTION:

% If we wouldn't be restricted by memory, the easiest version to
% create the variables us_at_L, vs_at_L, mt_S_L, md_S_L, it_S_L
% and id_S_L would be:

% dt = abs(repmat(tl,[nts 1]) - repmat(ts',[1 ntl]));
% [~,it_S_L_v] = min(dt,[],1);
% A.it_S_L = repmat(it_S_L_v, [ndl 1]);

% In the given example, dt has the dimensions
% [nts x ntl] = [10866 x 181689], so dt would take up
% approximately 16GB in the memory, so it is too big to be
% handled in this way.

% dz = abs(repmat(zl,[1 1 nds])-repmat(reshape(zs,[1 1 nds]),[ndl ...
   ndl 1]));
% [~,A.id_S_L] = min(dz,[],3);

% A.us_at_L = us(A.id_S_L, A.it_S_L);
% A.vs_at_L = vs(A.id_S_L, A.it_S_L);
% A.mt_S_L = abs(repmat(tl,[ndl 1]) - ts(A.it_S_L));
% A.md_S_L = abs(zl - zs(A.id_S_L));

%------------------------------------------------------------------
```

```
% PROGRAM VERSION TAKING INTO ACCOUNT MEMORY RESTRICTION:
% To account for the memory restriction, the upper program is
% broken up into smaller pieces of length np using a for loop.

A.it_S_L = NaN(ndl,ntl);
A.id_S_L = NaN(ndl,ntl);

% Choose np such that it fits the memory of the computer,
% while keeping the number of iterations in the loop as small as
% possible to allow for fast processing.
% (np probably approximately 10,000)

% Choose np for dt-loop:
np = ceil(memory/nts/8);

for ii = 1:ceil(ntl/np)
    disp(['Calculating ' num2str(ii) 'th iteration of ' num2str(...
        ceil(ntl/np)) ' iterations of the dt-loop.'])
    inds = (ii-1)*np + (1:np);
    inds = inds(inds <= ntl);
    dt = abs(repmat(tl(inds),[nts 1]) - repmat(ts',[1 length(inds)...
        ]));
    % dimensions of dt now: [nts x length(inds)]
    [~,it_S_L_v] = min(dt,[],1);
    A.it_S_L(:,inds) = repmat(it_S_L_v,[ndl 1]);
end % for ii = 1:ceil(ntl/np)

clear dt

% Choose np for dz-loop:
np = ceil(memory/(ndl*nds*8));

```

```
for ii = 1:ceil(ntl/np)
    disp(['Calculating ' num2str(ii) 'th iteration of ' num2str(...
       ceil(ntl/np)) ' iterations of the dz-loop.'])
    inds = (ii-1)*np + (1:np);
    inds = inds(inds <= ntl);
    dz = abs(repmat(zl(:,inds),[1 1 nds]) - repmat(reshape(zs,[1 1 ...
       nds]),[ndl length(inds) 1]));
    % dimensions of dz now: [ndl x length(inds) x nds]
    [~,A.id_S_L(:,inds)] = min(dz,[],3);
end % for ii = 1:ceil(ntl/np)

clear dz

A.us_at_L = us(sub2ind(size(us),A.id_S_L, A.it_S_L));
A.vs_at_L = vs(sub2ind(size(vs),A.id_S_L, A.it_S_L));
A.pgs_at_L = pgs(sub2ind(size(pgs),A.id_S_L, A.it_S_L));
A.mt_S_L = abs(repmat(tl,[ndl 1]) - ts(A.it_S_L));
A.md_S_L = abs(zl - zs(A.id_S_L));
A.el = el;

save([filedir filename],'A')
```

Listing 4: Sample code file `apply_ind.m`: It selects those LADCP and SADCP data points that pass a variety of selection criteria (compare Section 3.2.2).

```
% =================================================================
% PART 1:
% Program that reads the structures A in the
% SADCP_assigned_to_LADCP_dl.mat and SADCP_assigned_to_LADCP_ul.mat
% files (created by the script assign_SADCP_to_LADCP.m) into
% one structure A  with substructures AC(1) for the upward looking
% LADCP and AC(2) for the downward looking LADCP)

% PART 2:
% Program selects those data points that pass a variety of
% selection criteria (called ind)

% Last modified: 15 May 2015
% Created by: Dr. Wilken-Jon von Appen, Alfred Wegener Institute
% (AWI) & Joleen Heiderich (Jacobs University Bremen)

% ================================================================
% PART 1: CREATION OF STRUCTURE AC

% Loading of the SADCP_assigned_to_LADCP files and creation of
% structure AC:
SADCP_ul = 'D:\Meine Dokumente\Jacobs University Bremen\Bachelor ...
    Thesis\Matlab\Data\SADCP\SADCP_assigned_to_LADCP_ul.mat';
load(SADCP_ul)

AC(1) = A;

clear A

```

```
SADCP_dl = 'D:\Meine Dokumente\Jacobs University Bremen\Bachelor ...
    Thesis\Matlab\Data\SADCP\SADCP_assigned_to_LADCP_dl.mat';
load(SADCP_dl)

AC(2) = A;

filedir = 'D:\Meine Dokumente\Jacobs University Bremen\Bachelor ...
    Thesis\Matlab\Data\SADCP\';
filename = 'SADCP_assigned_to_LADCP.mat';

save([filedir filename],'AC')

% ===============================================================
% PART 2: APPLY INDEX CRITERIA

% Loading of the SADCP_assigned_to_LADCP.mat and the LADCP file:
SADCP = 'D:\Meine Dokumente\Jacobs University Bremen\Bachelor ...
    Thesis\Matlab\Data\SADCP\SADCP_assigned_to_LADCP.mat';
load(SADCP)

LADCP = 'D:\Meine Dokumente\Jacobs University Bremen\Bachelor ...
    Thesis\Matlab\Data\LADCP\LADCP_processing\processing\...
    L_one_vector.mat';
load(LADCP)
% The LADCP data has to be stored in a structure Lv with two
% substructures: Lv(1): upward looking LADCP,
% Lv(2): downward looking LADCP

% ---------------------------------------------------------------
% EXPLANATION OF THE DIFFERENT CUTOFF PARAMETERS AND THEIR
% DIMENSIONS:

```

```
% t_cutoff - cutoff value for the temporal minimum (if mt_S_L is
%            bigger than the cutoff, we cannot assign a SADCP
%            measurement value to the LADCP measurement);
%            Matlab date format, [1 x 1]
% d_cutoff - cutoff value for the vertical distance minimum (if
%            md_S_L is bigger than the cutoff, we cannot assign
%            a SADCP measurement value to the LADCP measurement);
%            in meters, [1 x 1]
% el_cutoff_m_s - cutoff value for the error velocity of the
%                 LADCP in meters per second (if el is bigger
%                 than the cutoff, we cannot assign a SADCP
%                 measurement value to the LADCP measurement);
%                 [1 x 1]
% el_cutoff_percent - cutoff value for the error velocity of the
%                     LADCP in percent(if el is bigger than the
%                     cutoff, we cannot assign a SADCP measurement
%                     value to the LADCP measurement); [1 x 1]
% pgs_cutoff - cutoff value for the percent good of the SADCP data
%              (if pgs is bigger than the cutoff, we cannot assign
%              a SADCP measurement value to the LADCP measurement);
%              in percent, [1 x 1]
% bl_cutoff - bottom depth determined from LADCP processing
%             routine,1 value for each cast (if the depth (Lv.z)
%             is bigger than the cutoff, we cannot assign a SADCP
%             measurement value to the LADCP measurement);
%             in meter, [1 x ntl]
% sur_cutoff - surface value (zero) + upper ocean layer that is
%              disregarded due to disturbance of the signal (if the
%              depth (Lv.z) is bigger than the cutoff, we cannot
%              assign a SADCP measurement value to the LADCP
%              measurement); in meter, [1 x 1]; negative depths are
%              found where bins are above the water surface
```

```
% s_min_cutoff - minimum speed (below this cutoff the LADCP cannot
%                 determine the current direction properly any more;
%                 in meters per second, [1 x 1]
% s_max_cutoff - maximum speed (possibility to exclude high
%                 velocities that occured only rarely;
%                 in meters per second, [1 x 1]

%----------------------------------------------------------------
% SET CUTOFF PARAMETERS:

t_cutoff = 1/24/60; % e.g. 1 minute
d_cutoff = 10; % e.g. 10 meter
el_cutoff_m_s = 0.02; % e.g. 0.02 meters per second
el_cutoff_per = 50; % e.g. 50%
pgs_cutoff = 90; % e.g. 90%
bl_cutoff = Lv(1).bot_dep_long - 20;
sur_cutoff = 60; % e.g. 60 m
s_min_cutoff = 0.04; %e.g. 0.04 meters per second
s_max_cutoff = 0.2; % e.g. 0.2 meters per second

%----------------------------------------------------------------
% IMPLEMENT CUTOFFS (DETERMINE INDICES TO USE AFTER REMOVING
% VALUES ABOVE THE CUTOFF)

for ii = 1:length(AC)
    % ii=2 (two structures of length 2 for upward and downward
    % looking LADCP/SADCP

    % Compute important values from SADCP & LADCP data:
        % speed_S: speed SADCP
        % dir_S: direction SADCP
        % speed_L: speed LADCP
```

```
        % dir_L: direction LADCP
        % head_L: heading LADCP
        % dS_dL_hL: correct heading
        % dS_dL: deviation between LADCP and SADCP
    % Note that for the direction the mathematical angle convention
    % is use here
    speed_S = sqrt((AC(ii).us_at_L).^2+(AC(ii).vs_at_L).^2);
    dir_S = atan2d(AC(ii).vs_at_L,AC(ii).us_at_L);
    speed_L = sqrt((Lv(ii).u).^2+(Lv(ii).v).^2);
    dir_L = atan2d((Lv(ii).v),(Lv(ii).u));
    head_L = repmat(mod(Lv(ii).heading+180,360)-180,[size(dir_S,1) ...
        1]); % 90-
    dS_dL_hL = mod(dir_S-dir_L+head_L+180,360)-180;
    dS_dL = mod(dir_S-dir_L+180,360)-180;

    % set indices for cutoffs (only good indices are taken)
    ind_t = AC(ii).mt_S_L < t_cutoff;
    ind_d = AC(ii).md_S_L < d_cutoff;
    ind_el_m_s = AC(ii).el < el_cutoff_m_s;
    ind_el_per = AC(ii).el./sqrt((Lv(ii).u).^2+(Lv(ii).v).^2)*100 <...
         el_cutoff_per;
    ind_pgs = AC(ii).pgs_at_L > pgs_cutoff;
    ind_bl = Lv(ii).z < repmat(bl_cutoff,[size(Lv(ii).z,1) 1]);
    ind_sur = Lv(ii).z > sur_cutoff;
    ind_spd = speed_S > s_min_cutoff & speed_S < s_max_cutoff  & ...
        speed_L > s_min_cutoff & speed_L < s_max_cutoff;
    ind_br_pr = Lv(ii).uvze_ind ~= 3 & Lv(ii).uvze_ind ~= 11 & Lv(...
        ii).uvze_ind ~= 19 & Lv(ii).uvze_ind ~= 23;
    % exclude profiles with non-synchronized times (3,11,19,23)
    ind = ind_t & ind_d & ind_el_m_s & ind_el_per & ind_pgs & ...
        ind_bl & ind_sur & ind_spd & ind_br_pr;

```

```
    % select speed, direction and heading values that passed the
    % index criteria
    speed_S_ind = speed_S(ind);
    dir_S_ind = dir_S(ind);
    speed_L_ind = speed_L(ind);
    dir_L_ind = dir_L(ind);
    head_L_ind = head_L(ind);
    dS_dL_hL_ind = dS_dL_hL(ind);
    dS_dL_ind = dS_dL(ind);
end
```

Table 1: Overview of the CTD stations in the Norske trough during the *R/V Polarstern* cruise PS85 on 14 June and 15 June 2014.

Station Name	**Latitude**	**Longitude**	**Water Depth**	**Time (UTC)**	**Projected Section Distance**
PS85/411-2	77° 43.062’ N	15° 28.693’ W	374 m	14 Jun 2014 14:00	5.71 km
PS85/412-1	77° 49.980’ N	14° 58.068’ W	447 m	14 Jun 2014 16:43	12.50 km
PS85/413-1	77° 46.320’ N	15° 11.113’ W	375 m	14 Jun 2014 18:19	19.56 km
PS85/414-1	77° 37.140’ N	15° 33.360’ W	334 m	14 Jun 2014 20:59	27.76 km
PS85/415-1	77° 32.328’ N	15° 40.188’ W	309 m	14 Jun 2014 22:23	36.69 km
PS85/416-1	77° 27.918’ N	15° 46.547’ W	305 m	14 Jun 2014 23:40	46.89 km
PS85/417-1	77° 25.572’ N	16° 02.791’ W	274 m	15 Jun 2014 00:56	55.65 km
PS85/418-1	77° 23.298’ N	16° 18.281’ W	170 m	15 Jun 2014 02:47	64.08 km
PS85/422-1	77° 55.482’ N	14° 36.019’ W	450 m	15 Jun 2014 16:43	77.27 km
PS85/423-1	77° 57.822’ N	14° 27.433’ W	402 m	15 Jun 2014 17:46	82.72 km
PS85/424-1	77° 59.640’ N	14° 16.602’ W	240 m	15 Jun 2014 18:55	87.82 km
PS85/425-1	78° 02.490’ N	14° 02.712’ W	133 m	15 Jun 2014 20:50	95.17 km

Table 2: Variables contained in the structure `l` created by the Lowered ADCP processing software *LADCP 2.0.0b* by C. Mertens (University of Bremen). Some data is collected seperately for uplooking and downlooking LADCP (marked by the number 4 in the dimensions) or even seperately for each of the four transducers of each instrument (marked by the number 2 in the dimensions).

Variable	Meaning	Unit	Dimension
updown	True for systems with up- & downward looking ADCPs		<1 x 1 logical>
scfg	Hardware configuration byte		<1 x 2 double>
nbin	Number of bins		<1 x 2 double>
npng	Number of pings per ensemble		<1 x 2 double>
blen	Bin length	m	<1 x 2 double>
blnk	Blank after transmit	m	<1 x 2 double>
dist	Distance to the middle of the first bin	m	<1 x 2 double>
plen	Pulse length	s	<1 x 2 double>
freq	Instrument frequency	kHz	<1 x 2 double>
zbin	Distance of depth cell centers from transducers	m	<1 x 2·nbin double>
ens	Ensemble number		<1 x 1 double>
tim	Time		<# of timesteps x 1 double>
sv	Sound velocity	m s^{-1}	<tim x 1 double>
s	Salinity	psu	<tim x 2 double>
t	Temperature	°C	<tim x 2 double>
hdg	Heading	°	<tim x 2 double>
pit	Pitch	°	<tim x 2 double>
rol	Roll	°	<tim x 2 double>

Table 2 continued.

Variable	Meaning	Unit	Dimension
u	Eastward velocity	m s^{-1}	<tim x 2·nbin double>
v	Northward velocity	m s^{-1}	<tim x 2·nbin double>
w	Vertical velocity	m s^{-1}	<tim x 2·nbin double>
e	Error velocity	m s^{-1}	<tim x 2·nbin double>
bs	Backscattering strength		<tim x 2·nbin double>
ei	Echo intensity		<tim x 2·nbin x # of transducers double>
cm	Correlation magnitude		<tim x 2·nbin x # of transducers double>
pg	Percent good		<tim x 2·nbin x # of transducers double>
hb	Bottom-track distance	m	<tim x 2·# of transducers double>
ub	Bottom-track east velocity	m s^{-1}	<tim x 2 double>
vb	Bottom-track north velocity	m s^{-1}	<tim x 2 double>
wb	Bottom-track vertical velocity	m s^{-1}	<tim x 2 double>
eb	Bottom-track error velocity	m s^{-1}	<tim x 2 double>
z	Depth of instrument	m	<tim x 2·nbin double>
hw	Water depth	m	<1x1 double>
ur	Reference layer eastward velocity	m s^{-1}	<timx2 double>
vr	Reference layer northward velocity	m s^{-1}	<timx2 double>
wr	Reference layer vertical velocity	m s^{-1}	<timx2 double>

Table 3: List of PS85 CTD and LADCP stations and errors that occured during LADCP processing. The CTD station number sometimes differs from the one written down on the CTD log sheet. The columns *CTD log sheet*, *Log sheet rosette*, $\delta^{18}O$ *log sheet* and 0_2 *sampling protocol* mark the stations for which log sheets are available for the different techniques. The column *Offset in raw data vertical velocity* indicates the stations at which the data was shifted for uplooking LADCP vs. downlooking LADCP in the raw data vertical velocity plot (compare Figure 11c) and the column *Bending in raw trace echo intensity* marks a strong bending down of the surface trace in the raw trace echo intensity plot (compare Figure 11f). The column *Non-sinusoidal compass deviation* refers to a random, non-sinusoidal in the compass deviation plot (compare Figure 10, 11a and 11b). The number of crosses describes how strongly the effect was visible (xxx means very pronounced). The columns *Empty bivariate histogram* marks the stations for which no LADCP data could be assigned to the SADCP data after applying the selection criteria, either for the uplooking LADCP or the downlooking LADCP or both (compare Section 3.2.2, Figures 14 and 15) and Listing 4. The stations highlighted in blue are located in the Norske trough.

Station name	**CTD station number** (+ Nr. on log sheet)	**LADCP station number**	**CTD log sheet**	**Log sheet rosette**	**δ^{18}O log sheet**	**0_2 sampling protocol**	**Offset in raw data vertical velocity**	**Bending in raw trace echo intensity**	**Non-sinusoidal compass deviation**	**Empty bivariate histogram**	**Comments**
401-01	1 (1)		x	x							No LADCP data
407-01	2 (2)		x	x							No LADCP data
411-02	3 (3)	1	x	x	x						
412-01	4 (4)	2	x	x	x						
413-01	5 (7)	3	x	x	x		x	xx	xxx		
414-01	6 (8)	4	x	x	x			x			
415-01	7 (9)	5	x	x	x						
416-01	8 (10)	6	x	x	x						
417-01	9 (11)	7	x	x	x			x			
418-01	10 (12)	8	x	x	x						SADCP switched on

Table 3 continued.

Station name	**CTD station number** (+ Nr. on log sheet)	**LADCP station number**	**CTD log sheet**	**Log sheet rosette**	**δ^{18}O log sheet**	**0_2 sampling protocol**	**Offset in raw data vertical velocity**	**Bending in raw trace echo intensity**	**Non-sinusoidal compass deviation**	**Empty bivariate histogram**	**Comments**
422-01	11 (13)	9	x	x	x						
423-01	12 (14)	10	x	x	x						
424-01	13 (15)	11	x	x	x		xxx	xxx	xxx		
425-01	14 (16)	12	x	x	x					uplooking & downlooking	Very wavy bottom trace in raw trace echo intensity plot
426-01	15 (17)	13	x	x	x						2 data files available: par & handpar
427-01	16 (18)	14	x	x	x						2 data files available: par & handpar; Broad signal in raw trace echo intensity plot
428-01	17 (19)	15	x	x	x						
429-01	18 (20)	16	x	x	x				x		Broad signal at the end in raw trace echo intensity plot
430-01	19 (21)	17	x	x	x				x		
431-01	20 (22)	18	x	x	x						

Table 3 continued.

Station name	**CTD station number** (+ Nr. on log sheet)	**LADCP station number**	**CTD log sheet**	**Log sheet rosette**	**δ^{18}O log sheet**	**0_2 sampling protocol**	**Offset in raw data vertical velocity**	**Bending in raw trace echo intensity**	**Non-sinusoidal compass deviation**	**Empty bivariate histogram**	**Comments**
432-01	21 (23)	19	x	x	x		xx	xx	xxx		Raw trace echo intensity plot: surface bends down bottom bends up
433-01	22 (24)	20	x	x	x				xx		Raw trace echo intensity plot: bottom trace slightly wavy
434-01	23 (25)	21	x	x	x					uplooking & downlooking	Broad, wavy signal at the end of raw trace echo intensity plot
435-01	24 (26)	22	x	x	x					uplooking & downlooking	
437-01	25 (27)	23	x	x	x		xxx	xxx	xxx		
438-01	26 (28)	24	x	x	x						
439-01	27 (29)	25	x	x	x				x		
440-01	28 (30)	26	x	x	x					uplooking & downlooking	
442-01	29 (31)	27	x	x	x						

Table 3 continued.

Station name	**CTD station number** (+ Nr. on log sheet)	**LADCP station number**	**CTD log sheet**	**Log sheet rosette**	**δ^{18}O log sheet**	**0_2 sampling protocol**	**Offset in raw data vertical velocity**	**Bending in raw trace echo intensity**	**Non-sinusoidal compass deviation**	**Empty bivariate histogram**	**Comments**
443-01	30 (32)	28	x	x	x	x				uplooking	Green curve in compass deviation plot (Figure 10); wrong time assignment, plot showing depth of instrument is not a function (Figure 11d)
444-01	31 (33)	29	x	x	x	x					
446-01	32 (34)	30	x	x	x	x					

Table 3 continued.

Station name	**CTD station number** (+ Nr. on log sheet)	**LADCP station number**	**CTD log sheet**	**Log sheet rosette**	**δ^{18}O log sheet**	**0_2 sampling protocol**	**Offset in raw data vertical velocity**	**Bending in raw trace echo intensity**	**Non-sinusoidal compass deviation**	**Empty bivariate histogram**	**Comments**
447-01	33 (35)	31	x	x	x	x					3 data files available: 447-01.par, 447-01-no-redt.par (editing threshold set to zero) 447-01-smaller-depth-cell.par (depth cell set to 4 instead of 10); raw trace echo intensity plot cannot be created for 447-01-no-redt.par
448-01	34 (36)	32	x	x	x	x					
449-01	35 (37)	33	x	x	x	x					
455-02	36 (38)	34	x	x							
456-01	37 (39)	35		x		x					CTD log sheet is missing

Table 3 continued.

Station name	**CTD station number** (+ Nr. on log sheet)	**LADCP station number**	**CTD log sheet**	**Log sheet rosette**	**δ^{18}O log sheet**	**0_2 sampling protocol**	**Offset in raw data vertical velocity**	**Bending in raw trace echo intensity**	**Non-sinusoidal compass deviation**	**Empty bivariate histogram**	**Comments**
465-01	39 (41)	37	x	x	x	x					Very deep station (6000 m), offset and bending cannot be seen anymore
469-01	40 (42)	38	x	x	x	x					
470-01	41 (43)	39	x	x							
473-01	42 (44)	40		x							CTD log sheet is missing
473-06	43 (45)	41	x	x		x					CTD set-up changed to configuration 4; double surface and no bottom trace in raw trace echo intensity plot (LADCP only went to 550 m depth, station depth is 2600 m)
481-06	44 (46)	42	x	x	x	x					
482-01	45 (47)	43	x	x	x	x					CTD log sheet has notes on backside

Table 3 continued.

Station name	**CTD station number** (+ Nr. on log sheet)	**LADCP station number**	**CTD log sheet**	**Log sheet rosette**	**δ^{18}O log sheet**	**0_2 sampling protocol**	**Offset in raw data vertical velocity**	**Bending in raw trace echo intensity**	**Non-sinusoidal compass deviation**	**Empty bivariate histogram**	**Comments**
483-01	46 (48)	44	x	x	x						
484-01	47 (49)	45	x	x							
485-01	48 (50)	46	x	x							
486-01	49 (51)	47	x								
490-01	50 (52)	48	x	x							
491-01	51 (53)	49	x	x							
492-01	52										No LADCP data; CTD log sheet is missing (instead a CTD log sheet for non-existent CTD station 491-02 is available)
493-01	53		x								No LADCP data

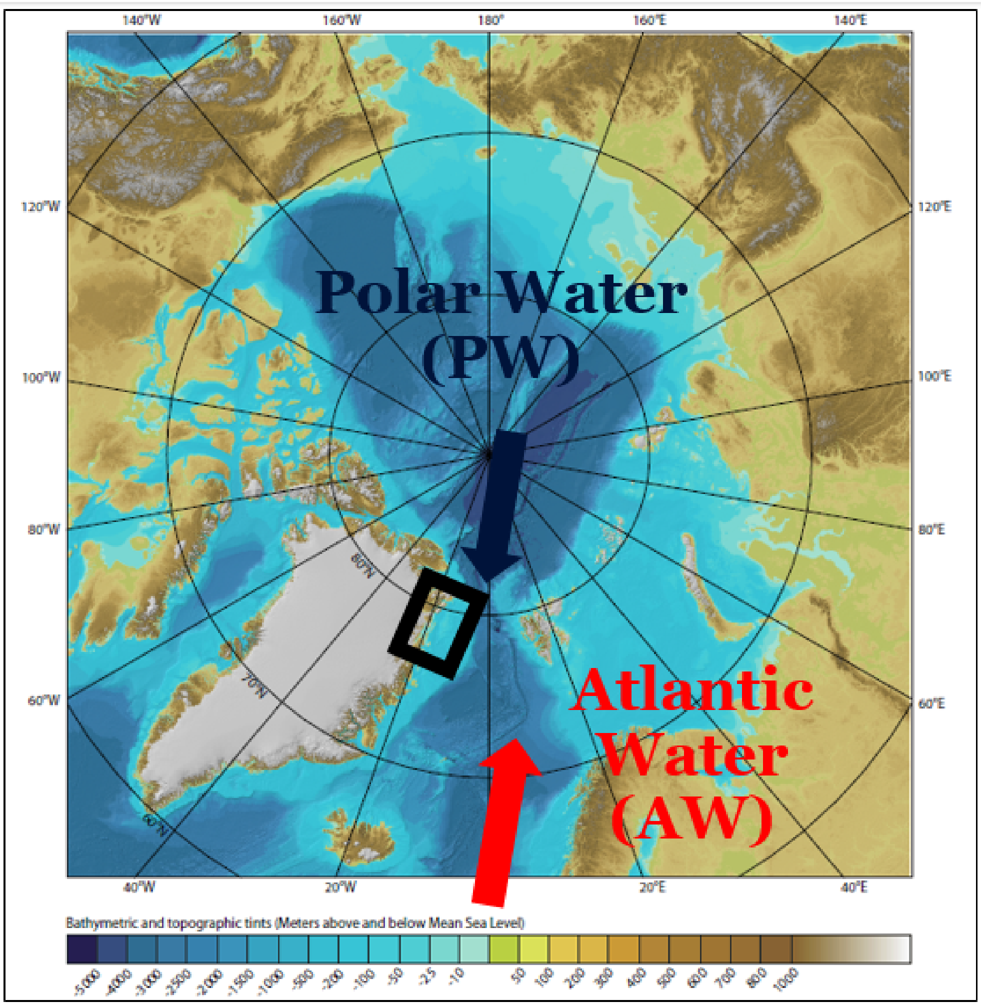

Figure 1: Polar stereographic bathymetric map of the Arctic. The blue and red arrows schematically depict the origin of two distinct water masses characterizing the flow on the East Greenland Shelf: cold, fresh Polar Water (PW) and warm, saline Atlantic Water (AW). The black box indicates the region investigated in this project (see Figure 2). (Adapted from the International Bathymetric Chart of the Arctic Ocean (IBCAO) Version 3.0 (Jakobsson et al., 2012))

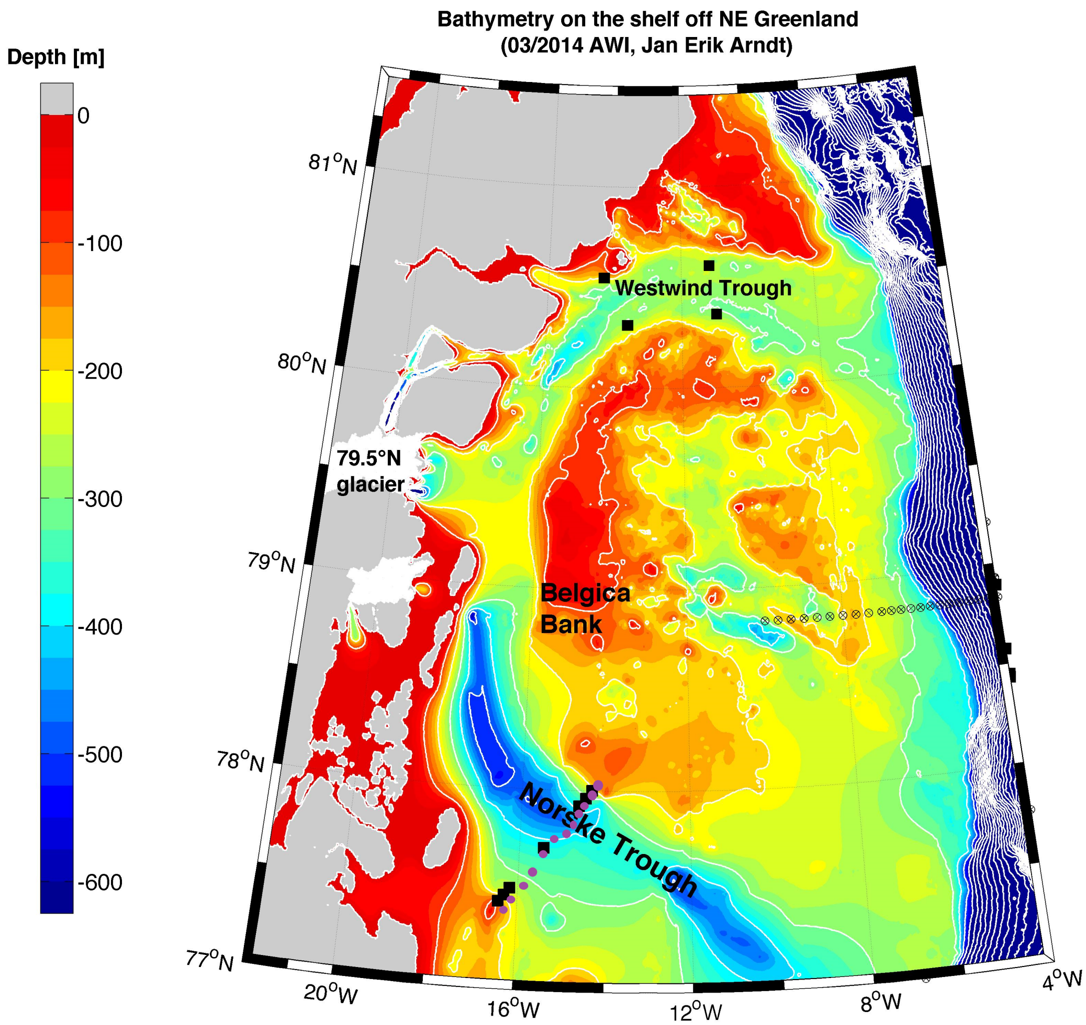

Figure 2: Bathymetric map of the North East Greenland Shelf based on the International Bathymetric Chart of the Arctic Ocean (IBCAO) Version 3.0 (Jakobsson et al., 2012) with an improved interpretation as in Arndt et al. (2015). The extent is shown by the black box in Figure 1. The Nioghalvfjerdsfjorden glacier is indicated at 79.5° N. Black squares mark the positions of moorings. The mooring array in the Westwind trough (black squares) was deployed in late July and early August 1992 and recovered approximately one year later. The Norske trough mooring array (black squares) was deployed in June 2014 and has not been recovered yet. The purple dots indicate the positions of CTD casts conducted on the *R/V Polarstern* cruise PS85 in June 2014. (Adapted from Arndt et al. (2015))

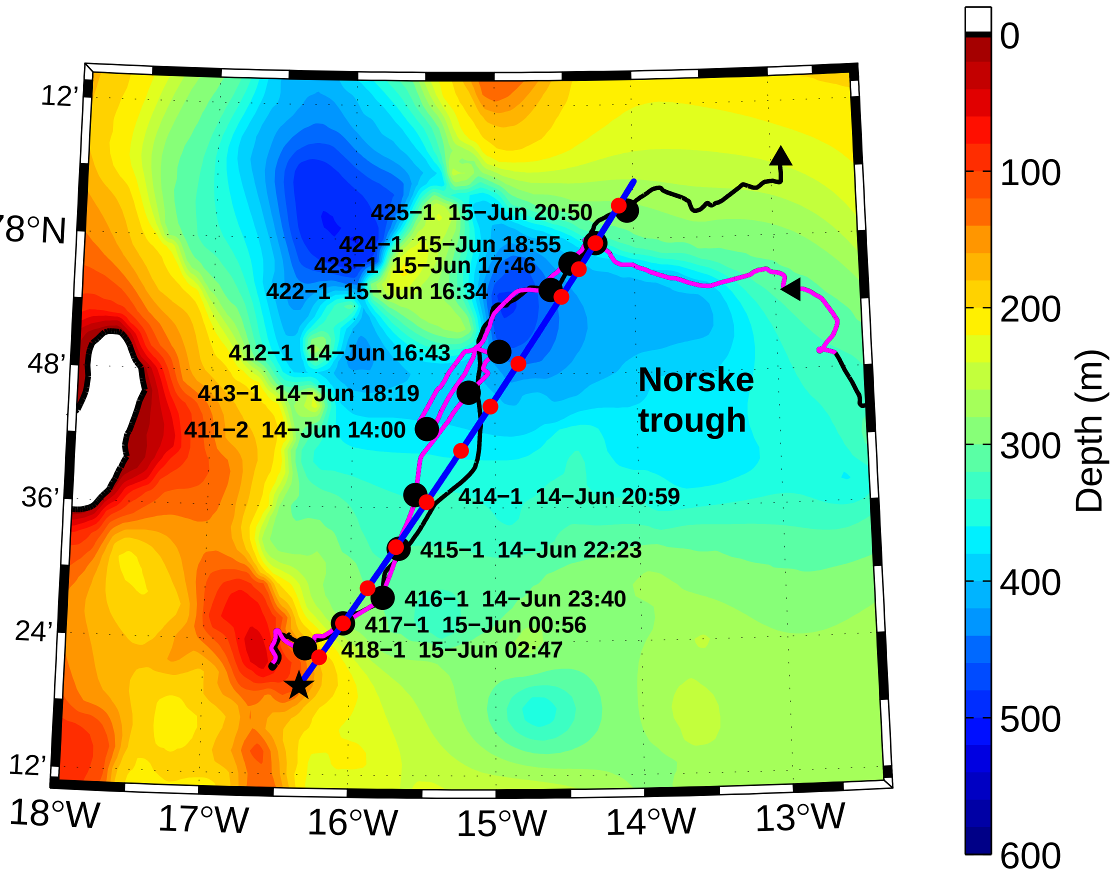

Figure 3: Zoomed bathymetric map of the North East Greenland Shelf based on the International Bathymetric Chart of the Arctic Ocean (IBCAO) Version 3.0 (Jakobsson et al., 2012). The black line represents the ship track on 14 June 2014 and 15 June 2014 during PS85 with the stations indicated as black dots. The transect was orthogonally projected onto the blue line, which ranges from zero section distance to 100 km section distance. The location 77° 19.908' N 16° 20.418' W is defined as zero section distance. The red dots mark the projected station locations. The pink line shows the part of the track for which the SADCP velocities were investigated. The black triangle marks the direction in which the ship moved during the transect.

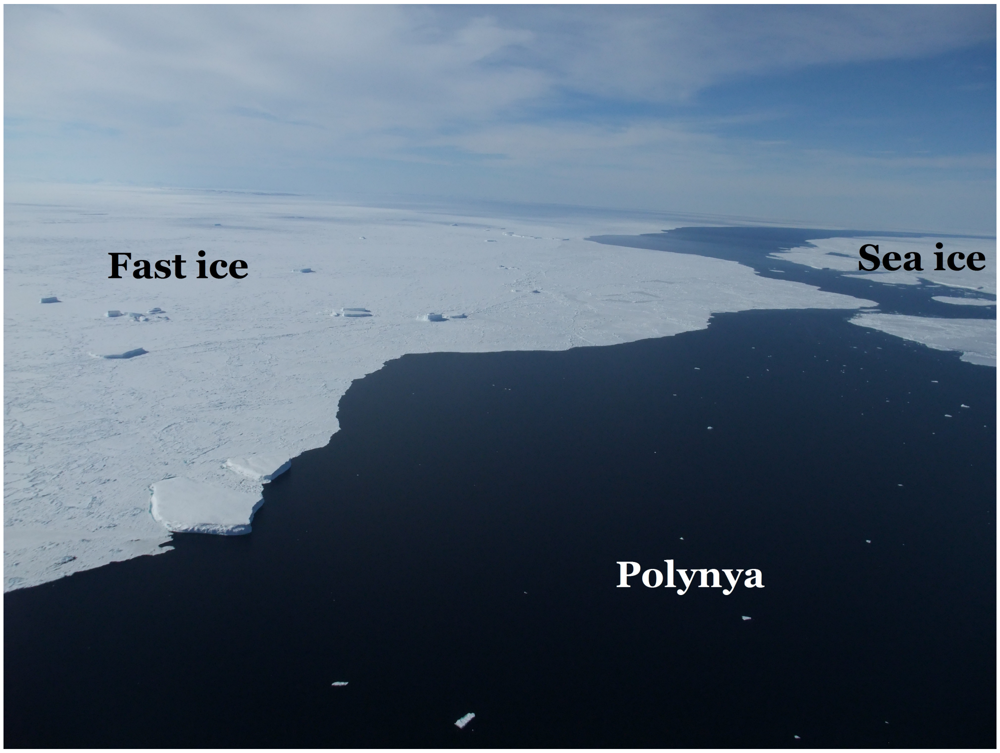

Figure 4: The polynya in the Norske trough where the CTD casts were taken. Photo from aerial reconnaissance flight during *R/V Polarstern* cruise PS85. The view is towards northeast. The shore and the Nioghalvfjerdsfjorden glacier, the source of the icebergs in the fast ice, are located to the left. (Photo by W.-J. von Appen, Alfred Wegener Institute)

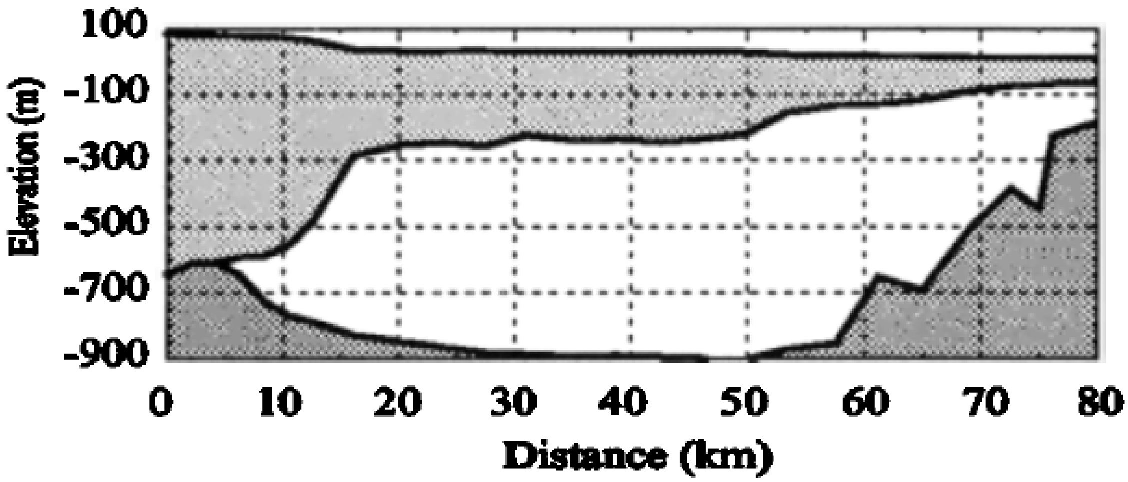

Figure 5: Cross-section of the floating ice-tongue of the marine terminating glacier Nioghalvfjerdsfjorden at 79.5° N. Best estimate of ice thickness and ocean bottom depth from a longitudinal seismic profile. (Adapted from Mayer et al. (2000))

Figure 6: CTD, rosette and LADCPs on board *R/V Polarstern*. The yellow LADCPs, one facing upward and one facing downward, are mounted onto the rosette and measure flow speed and direction simultaneouly to every CTD cast. The middle yellow pot is an additional battery pack for the LADCP system. A big steel weight is located inside the rosette (not visible here). (Photo: T. Dippe, Alfred Wegener Institute)

UNS S32760 / 1.4501 / F55

DATA SHEET

SUPER DUPLEX STAINLESS STEEL

TYPICAL APPLICATIONS

Pumps, valves, chokes, Xmas trees, pipework / flanges, bolting, connectors & manifolds. In oil and gas industry. Equipment in defence, chemical and marine industries.

PRODUCT DESCRIPTION

Material to UNS S32760 (and the other specifications listed below) is described as a super duplex stainless steel with a microstructure of 50:50 austenite and ferrite. The steel combines high mechanical strength (typically up to 600 MPa yield strength) and good ductility with outstanding corrosion resistance to marine environments and a wide, diverse range of oil & gas production environments. The alloy is supplied with a PREn (Pitting Resistance Equivalent) at >40.0 which guarantees high resistance to pitting corrosion. In addition, the steel offers high resistance to crevice corrosion and stress corrosion cracking. Ambient and subzero (down to minus 50^0C) notch ductility is good. These attributes mean that this super duplex steel can be used successfully as an alternative to 300 series stainless steel (such as type 316), standard 22% Cr duplex steel and precipitation hardening stainless steels. Where appropriate the alloy can be considered in lieu of more costly Grade 5 titanium or nickel based alloys.

AVAILABILITY

Bar, forgings, sheet, plate, pipe, tube, closed die forgings, flanges and welding consumables.

MATERIAL SPECIFICATIONS

- UNS S32760 in various ASTM product form specifications
- EN 10088-3 1.4501 (Grade X2CrNiMoCuWN25-7-4)
- NORSOK MDS D51 to D55, D57 & D58
- ASTM A182 F55
- NACE MR01-75 (latest revision) / ISO 15156

MACHINABILITY / WELDING

The machining and welding of this grade of super duplex stainless steel presents no particular problems. Guidance notes are available upon request.

CHEMICAL COMPOSITION %

Weight (%)	C	Mn	Si	S	P	Cr	Ni	Mo	Cu	N	W	PREn
Min.						24.0	6.0	3.0	0.50	0.20	0.50	40.0
Max	0.03	1.00	1.00	0.015	0.035	26.0	8.0	4.0	1.00	0.30	1.00	

PREn = Cr % + 3.3Mo% + 16N%

MINIMUM MECHANICAL PROPERTIES AT ROOM TEMPERATURE (EN 10088-3 1.4501 MAX DIAMETER 160mm – SOLUTION TREATED)

Ultimate Tensile Strength	730 – 930 MPa	(106 – 135 ksi)
0.2% Proof Strength	530 MPa	(77 ksi)
Elongation	25 %	
Hardness (Max)	290 HB	
Impact	100 J	(74 ft.lb)

TYPICAL PHYSICAL PROPERTIES

Density	7.8	kg/dm^3
Specific Thermal Capacity at 20^0C	500	$J.Kg^{-1}.K^{-1}$
Mean Coefficient of Thermal Expansion at 20 - 100^0C	13.0	$x\ 10^{-6}\ K^{-1}$
Thermal Conductivity at 20^0C	15	$W.m^{-1}.K^{-1}$
Electrical Resistivity at 20^0C	0.80	$\Omega\ .mm^2\ .m^{-1}$
Modulus of Elasticity at 20^0C	200	GPa
Magnetisable	Yes	

TECHNICAL SALES ASSISTANCE

Our resident team of qualified metallurgists and engineers will be pleased to assist further on any technical topic.

Smiths High Performance
Unit O, Stratton Business Park, London Road, Biggleswade, Bedfordshire SG18 8QB United Kingdom
Tel: +44 (0) 1767 604 708 Fax: +44 (0) 01767 312 885 Email: sales@smithshp.com Website: www.smithshp.com

All information in this data sheet is based on approximate testing and is stated to the best of our knowledge and belief. It is presented apart from contractual obligations and does not constitute any guarantee of properties or of processing or application possibilities in individual cases. Our warranties and liabilities are stated exclusively in our terms of trading. *© Smiths Metal Centres Ltd 2007*

Figure 7: Material data sheet for the steel used in the steel weight in the CTD rosette of *R/V Polarstern*. The super duplex stainless steel has a microstructure of 50:50 austenite and ferrite and is magnetizable according to the data sheet. File downloaded from `http://www.smithmetal.com/downloads/stainless_datasheets.htm`.

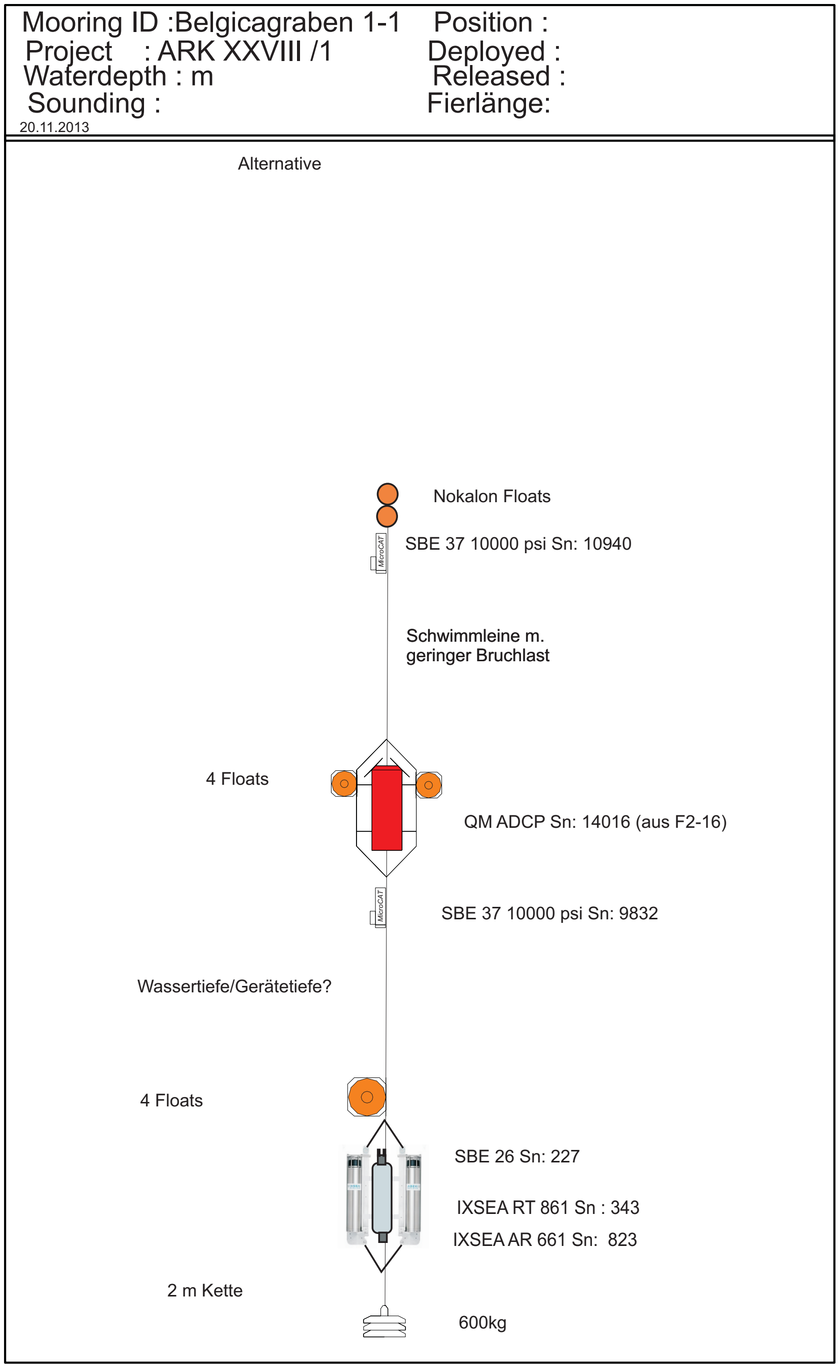

Figure 8: Mooring design drawing of one of the AWI moorings in the Norske trough deployed on 14 June and 15 June 2014 between 7° 23.388' N 16° 17.832' W and 77° 59.850' N 14° 18.612' W. (Credits: M. Monsees, Alfred Wegener Institute)

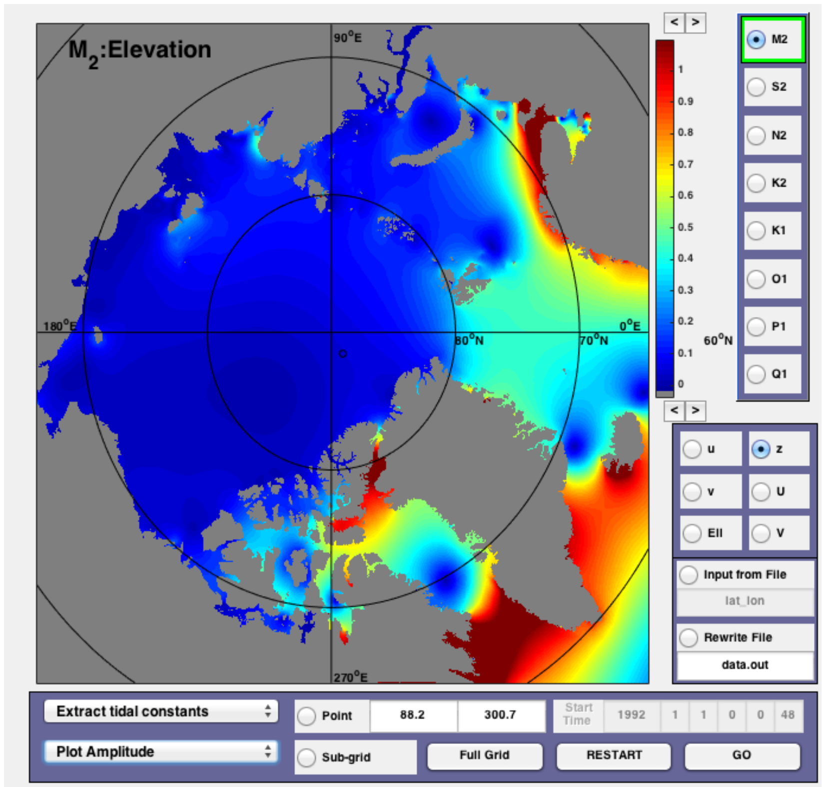

Figure 9: The graphical user interface (GUI) of the AOTIM5 model, a barotropic tidal model of the Arctic Ocean. It allows the user to extract the tidal constants (eastward velocity amplitude u, northward velocity amplitude v and tidal elevation amplitude z) for the major tides M_2, S_2, N_2, K_2, K_1, O_1, P_1 and Q_1 at a selected location (Padman and Erofeeva, 2004).

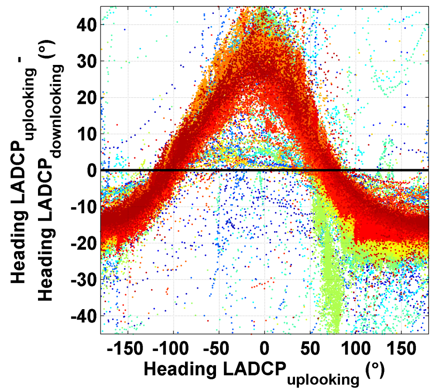

(a)

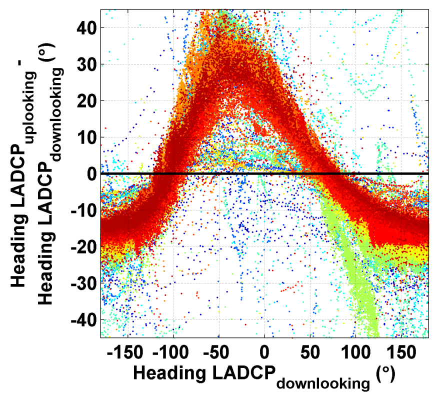

(b)

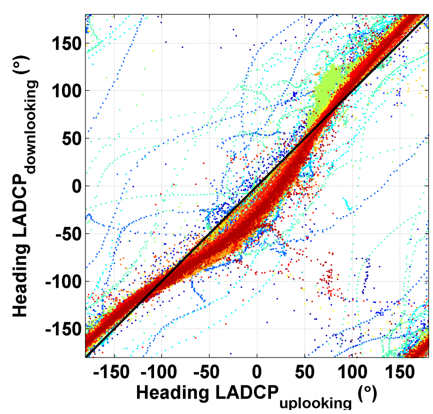

(c)

Figure 10: (a) Compass deviation shown as the difference between the upward and the downward looking LADCP headings as a function of the upward looking LADCP heading. (b) Analogous to (a), but shown as a function of the downward looking LADCP heading. (c) Heading deviations of the downward looking LADCP vs. the upward looking LADCP.
The black lines indicate the idealized expected data scatter if both the upward looking and the downward looking LADCPs measured the same headings.

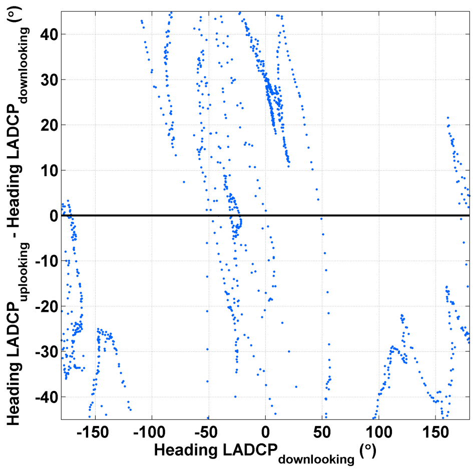

(a)

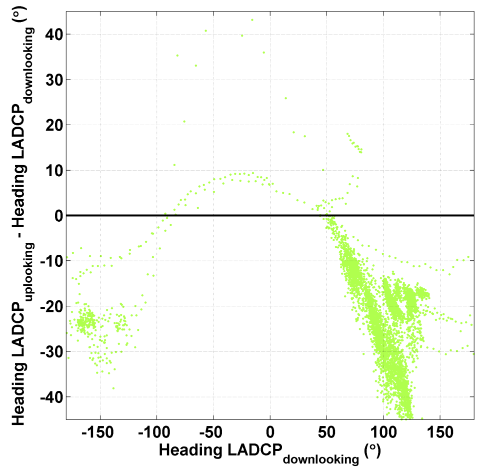

(b)

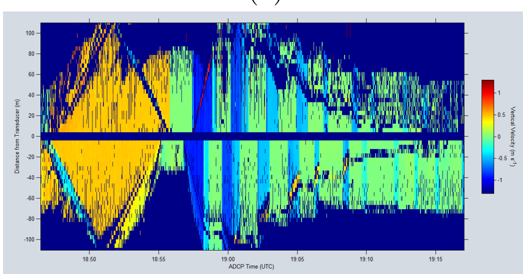

(c)

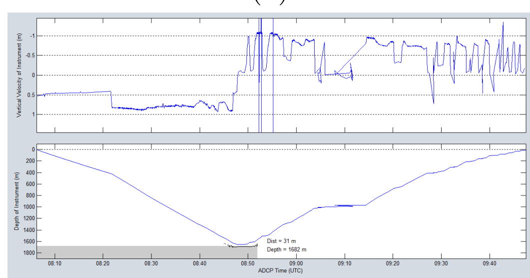

(d)

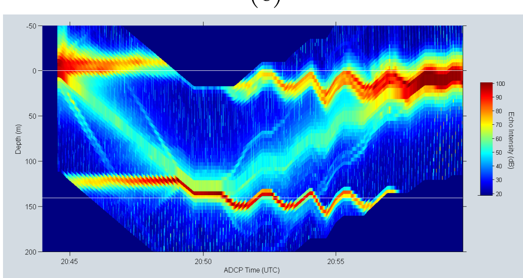

(e)

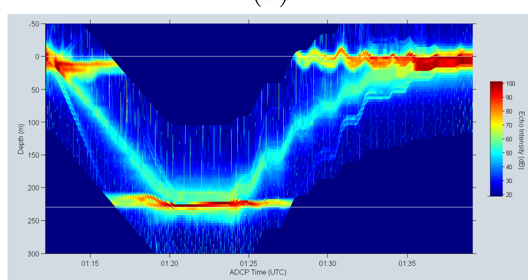

(f)

Figure 11: Errors that occurred during the processing of the LADCP data.
(a) Station 424-01: Random, non-sinusoidal signal in compass deviation plot (compare Figure 10)
(b) Station 443-01: Green signal in compass deviation plot (coincides with d, compare Figure 10)
(c) Station 424-01: Temporal offset in raw data vertical velocity for upward looking and downward looking LADCP
(d) Station 443-01: Erroneous time assignment, depth vs. time plot is not a function (coincides with b)
(e) Station 425-01: Very wavy bottom trace in raw trace echo intensity plot
(f) Station 432-01: Bending of surface trace in raw trace echo intensity plot

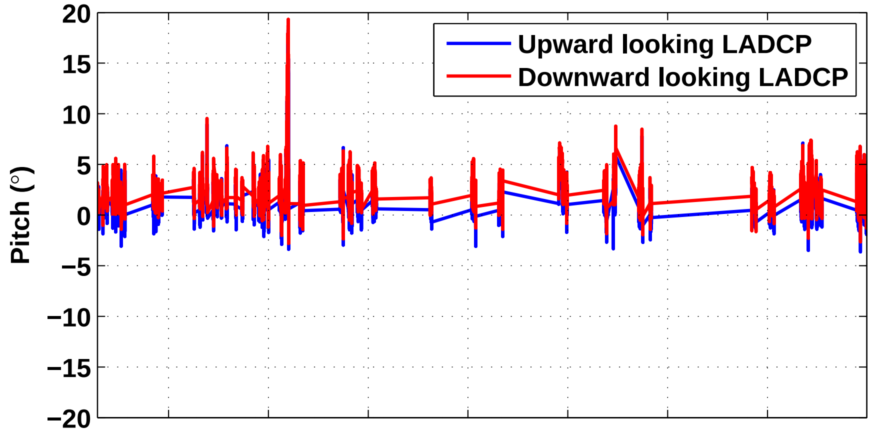

(a)

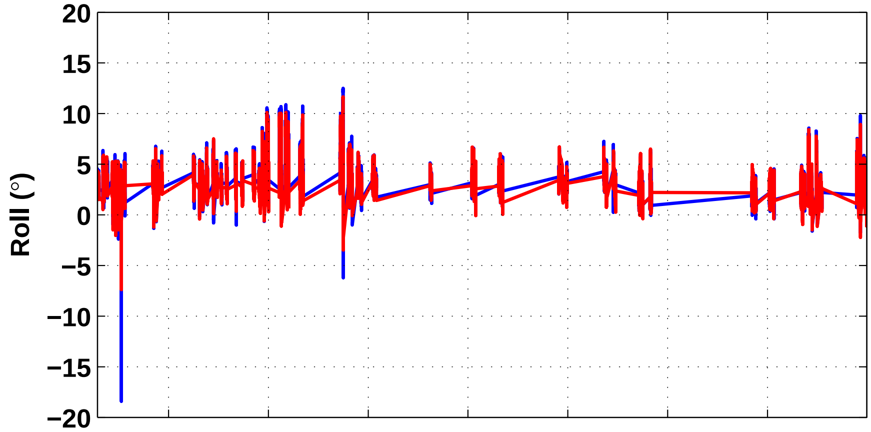

(b)

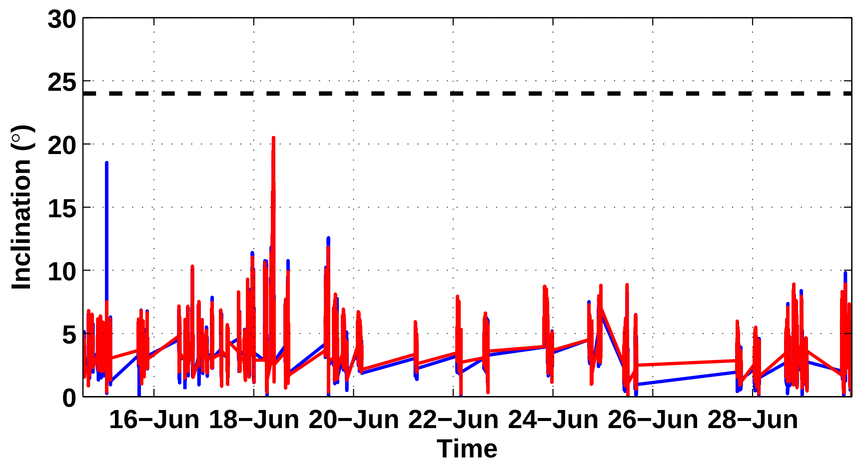

(c)

Figure 12: Pitch (a), roll (b) and inclination (c) recorded by the upward looking LADCP (blue) and the downward looking LADCP (red) during the *R/V Polarstern* cruise PS85. Dashed lines indicate the maximum recordable inclination threshold of 24°.

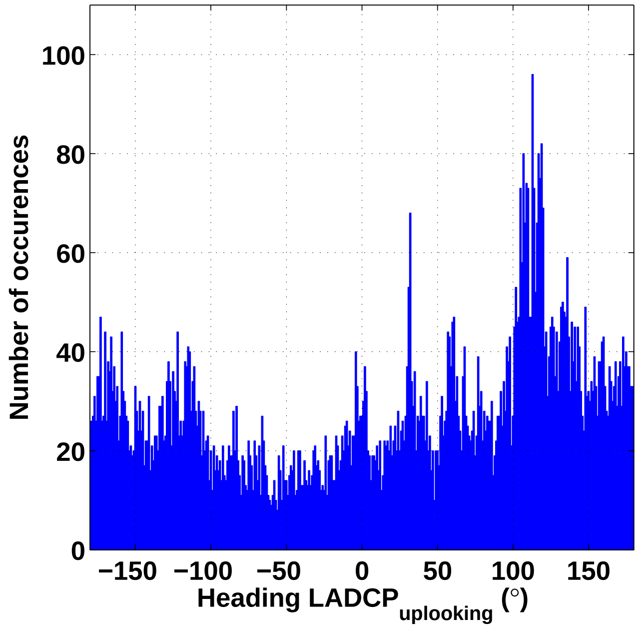

(a)

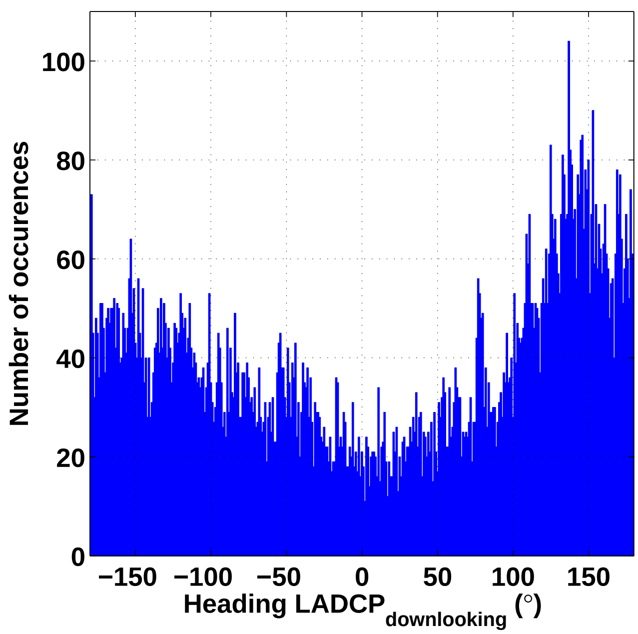

(b)

Figure 13: Histograms showing the headings recorded by the upward looking LADCP (a) and the downlooking LADCP (b) during the *R/V Polarstern* cruise PS85. The heading measurements shown here passed the selection criteria explained in Section 3.2.2 and Listing 4.

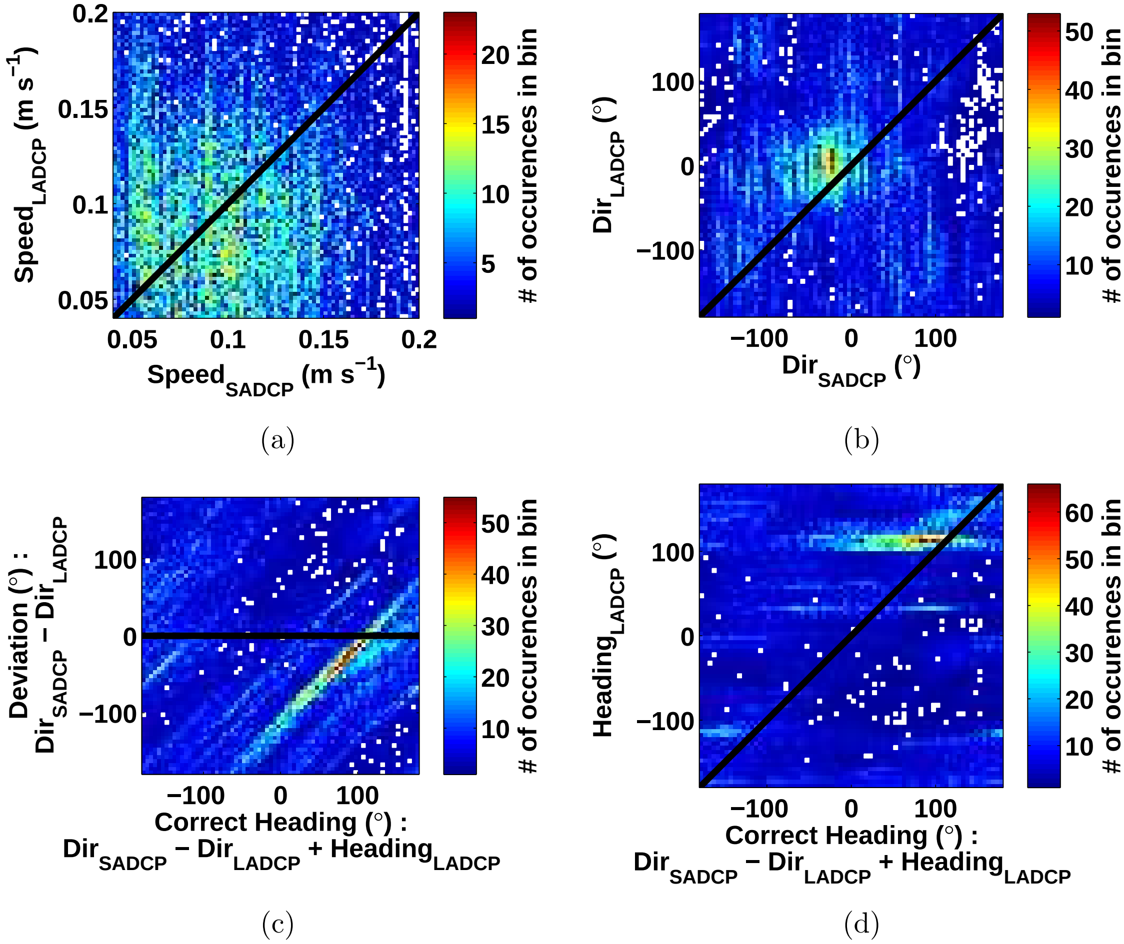

Figure 14: Bivariate histograms of upward looking LADCP and SADCP data. Black lines show the expected location of the data points if SADCP and LADCP would have recorded exactly the same current velocity values and if the LADCP heading was corrected appropriately.
(a) Current speed measured by the upward looking LADCP vs. current speed measured by the SADCP.
(b) Current direction measured by the upward looking LADCP vs. current speed measured by the SADCP.
(c) Deviation between the current direction measurements of SADCP and upward looking LADCP vs. corrected LADCP heading.
(d) Measured LADCP heading vs. corrected LADCP heading.

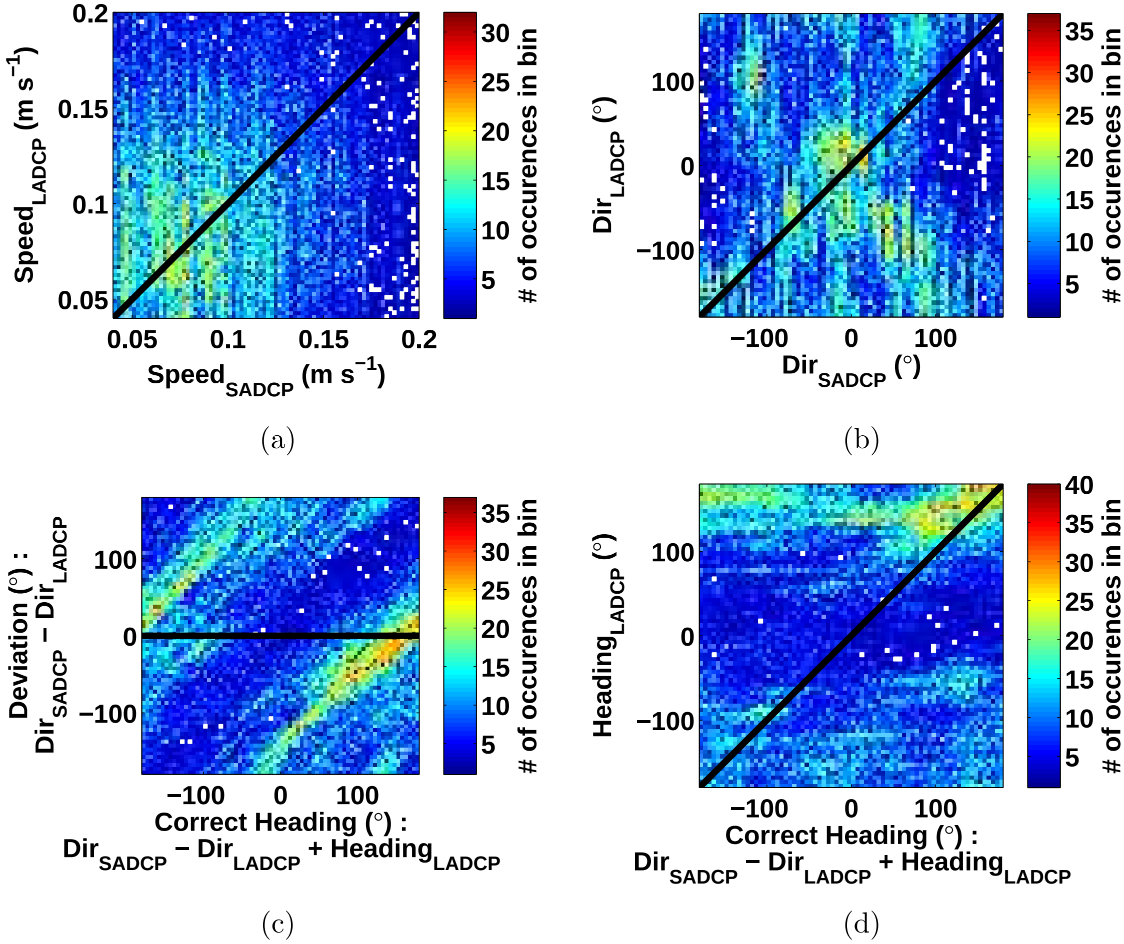

Figure 15: Bivariate histograms of downward looking LADCP and SADCP data, analogous to Figure 14.

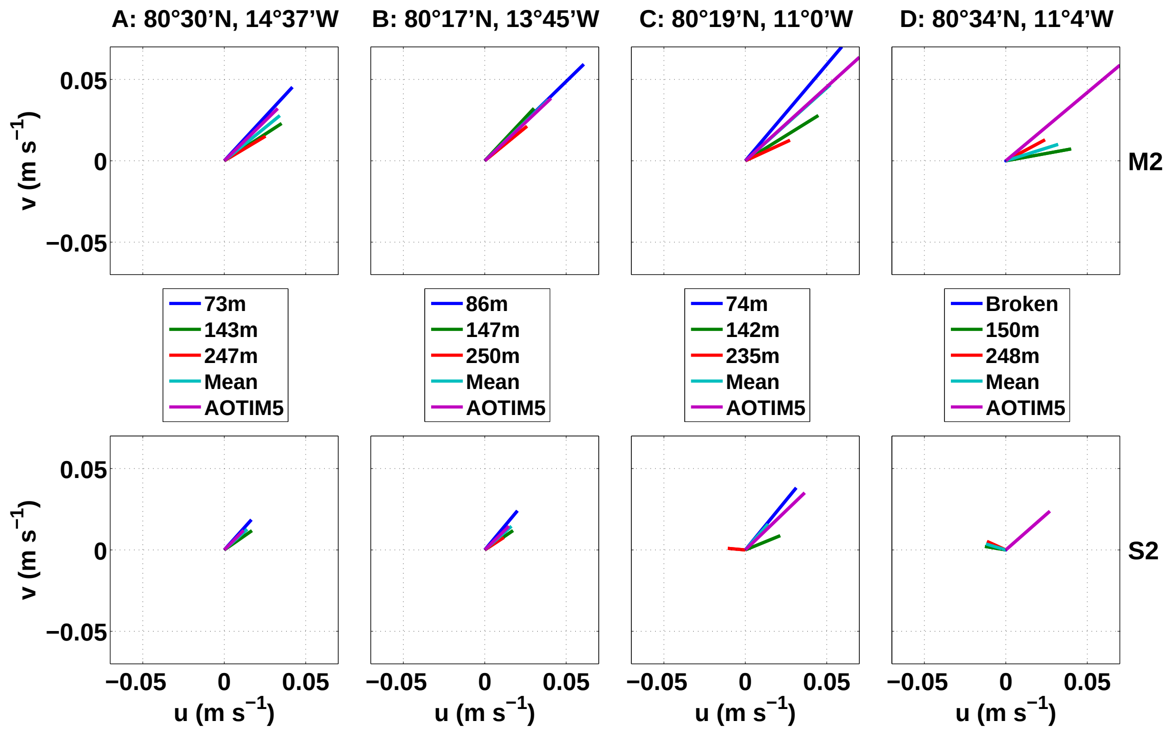

Figure 16: Magnitude and direction (eastward velocity u vs. northward velocity v) of the tidal flow at the location of the moorings A, B, C and D in the Westwind trough. Upper row: M_2 tide. Lower row: S_2 tide. Blue, red and green indicate the tidal components determined from current meter time series at three different depths using the harmonic tidal analysis of *t_tide* (Pawlowicz et al., 2002). Light blue shows the mean tidal flow of all the current meters for each mooring. Purple are the tidal predictions based on the barotropic model AOTIM5. The upper current meter in mooring D was broken and did not record a time series.

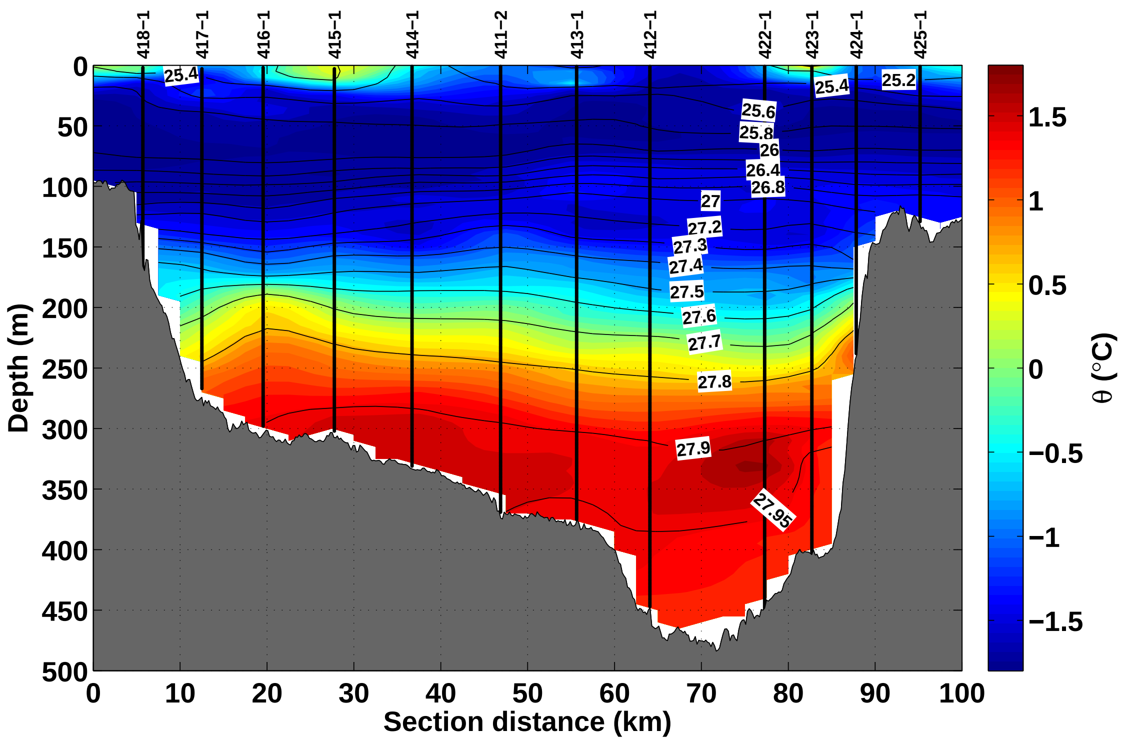

Figure 17: CTD transect showing potential temperature θ in the Norske trough, based on measurements taken during the *R/V Polarstern* cruise PS85 on 14 June and 15 June 2014. Bold black lines indicate the location of the 12 individual CTD casts and thin black contour lines represent isopycnals. The gidding was done with cubic splines under tension (Smith and Wessel, 1990). The bathymetry shown is based on 200-m averages of the echosounder data collected during all three crossings of the trough.

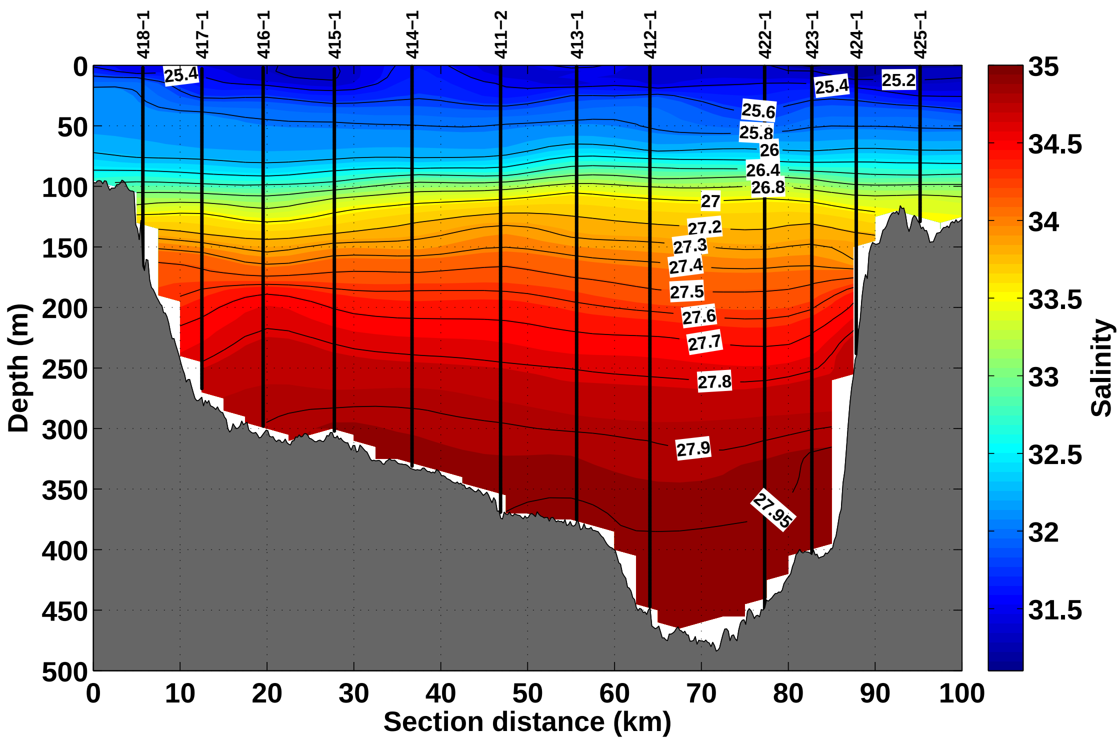

Figure 18: CTD transect showing salinity in the Norske trough, analogous to Figure 17.

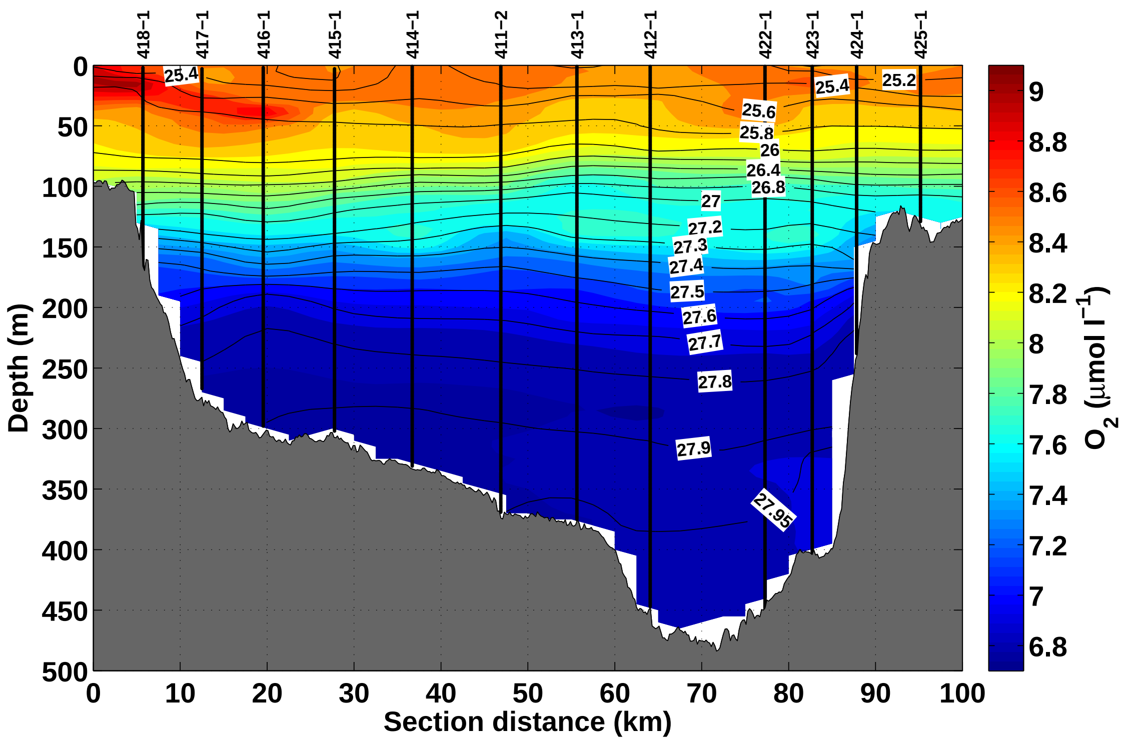

Figure 19: CTD transect showing oxygen concentration in the Norske trough, analogous to Figure 17.

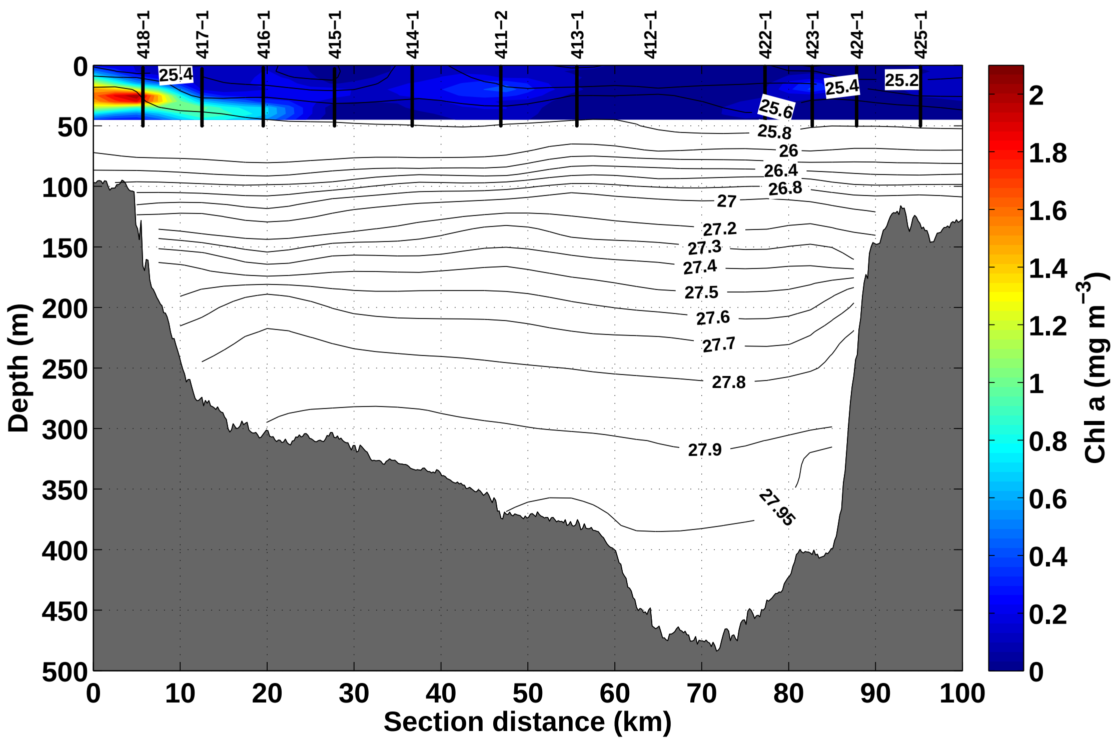

Figure 20: CTD transect showing chlorophyll *a* concentration in the Norske trough, analogous to Figure 17.

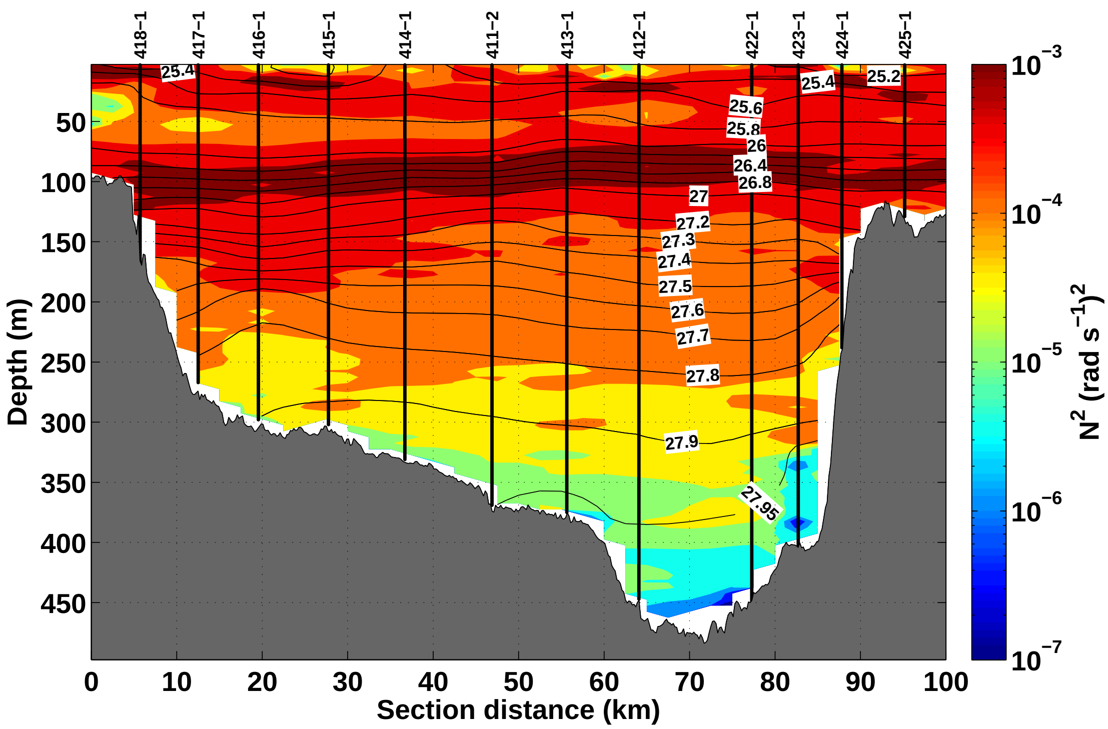

Figure 21: CTD transect showing buoyancy frequency squared N^2 in the Norske trough, analogous to Figure 17. Note the logarithmic color scale.

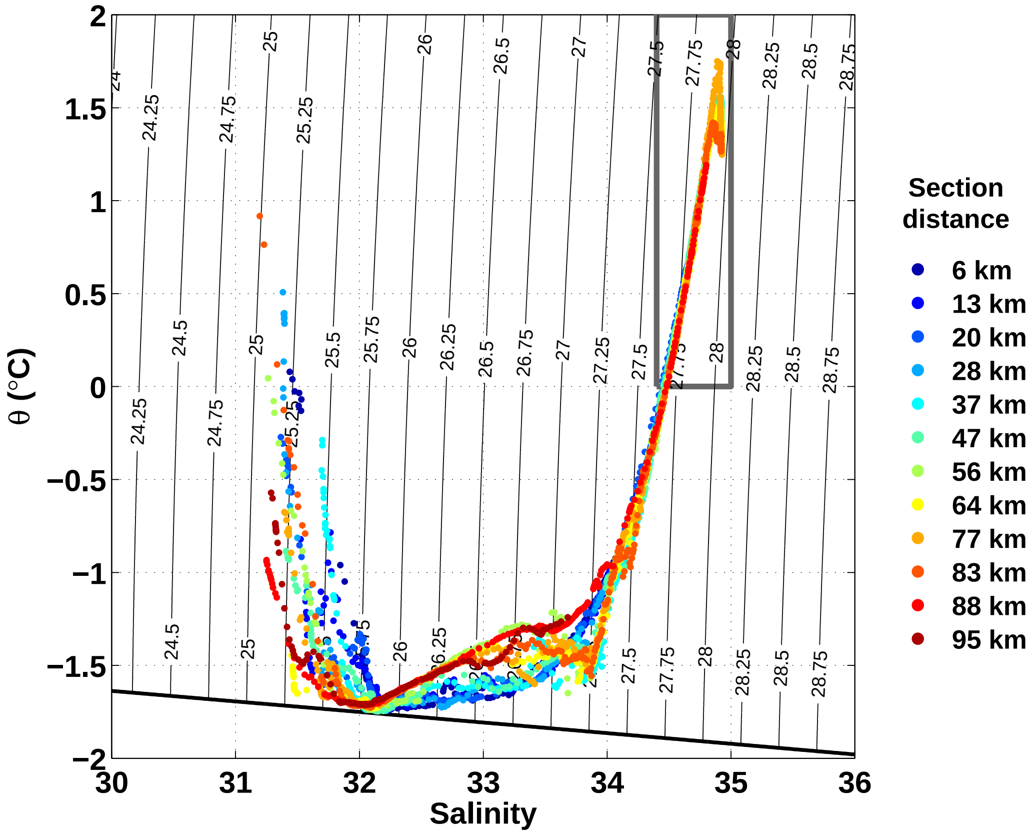

Figure 22: θ-S plot showing the water masses in the Norkse trough colored by section distance of the CTD stations taken during the *R/V Polarstern* cruise PS85 on 14 June and 15 June 2014. The thin black lines represent isopycnals and the bold line shows the freezing line of sea water. The gray box indicates the extent of the plot that is shown in Figure 23.

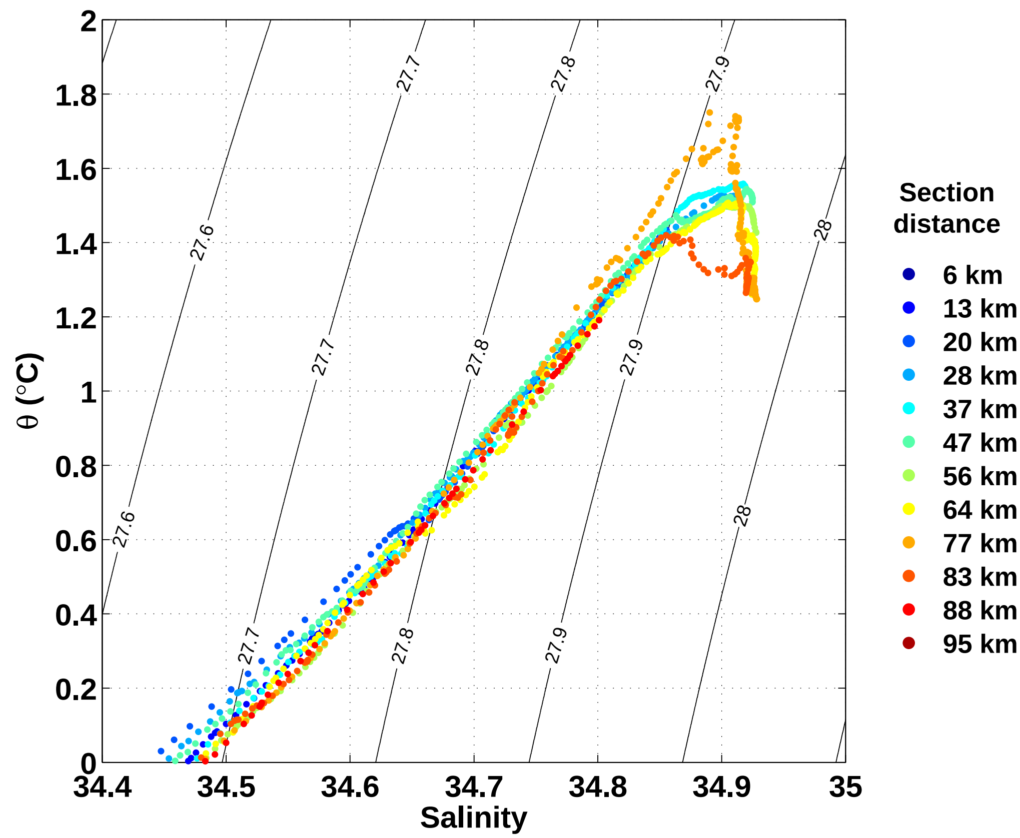

Figure 23: θ-S plot, zoomed version of Figure 22 (indicated by the gray box).

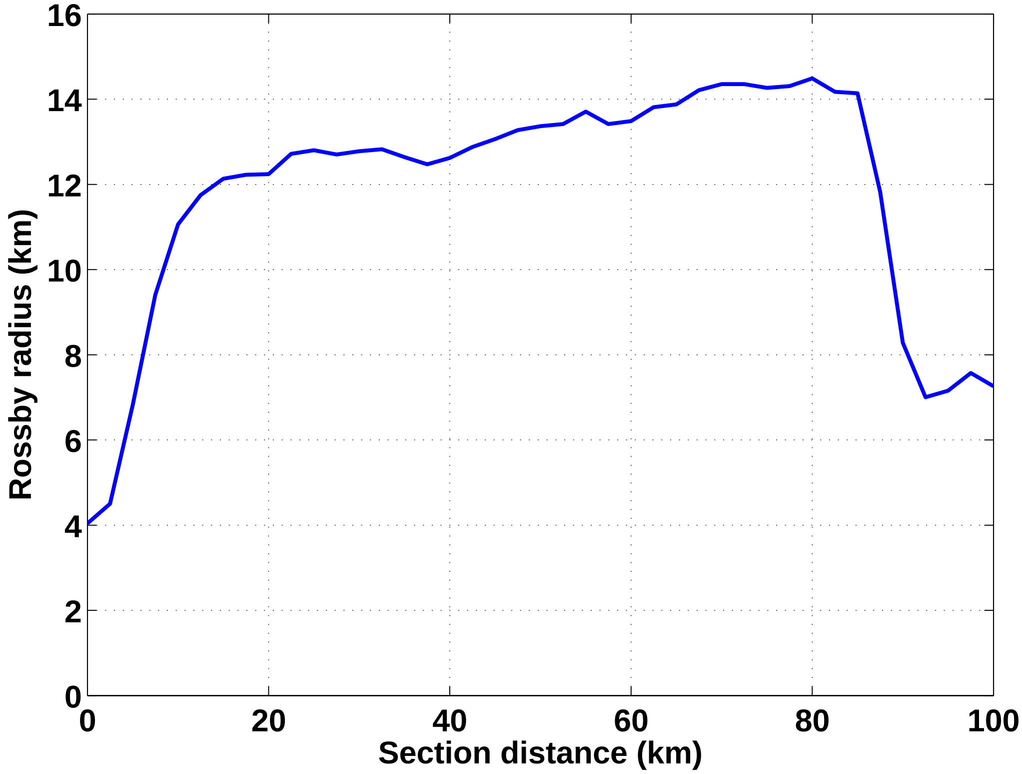

Figure 24: Rossby radius along the Norske trough transect calculated from CTD measurements conducted during the *R/V Polarstern* cruise PS85 on 14 June and 15 June 2014.

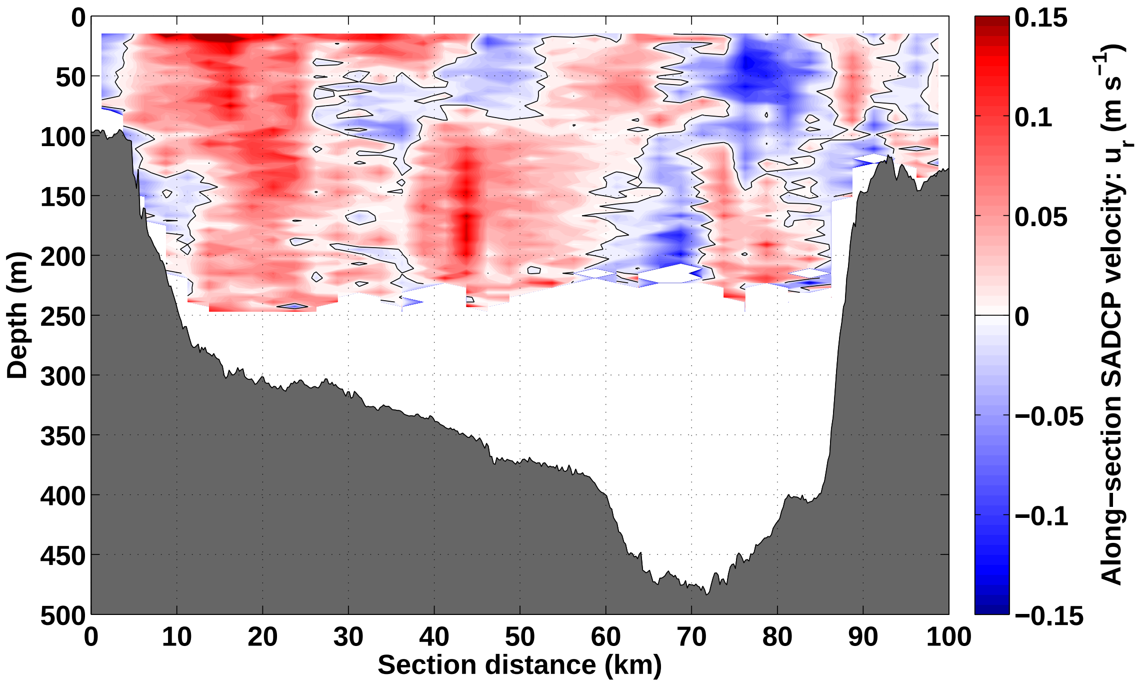

Figure 25: Along-section velocity u_r in the upper 250 m in the Norske trough as measured by the SADCP on *R/V Polarstern* cruise PS85 from 14 June 2014 01:00 UTC and 15 June 2014 04:15 UTC (indicated by the pink transect in Figure 3). Thin black lines represent the zero velocity contour. The bathymetry shown is based on 200-m averages of the echosounder data collected during all three crossings of the trough.

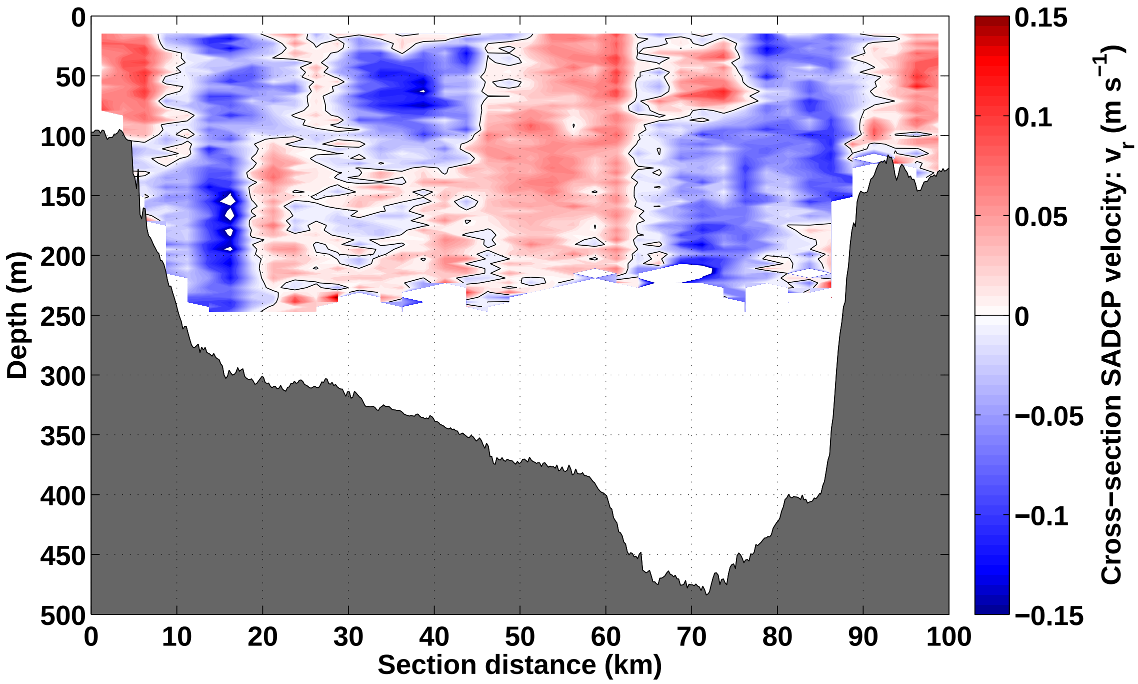

Figure 26: Cross-section velocity v_r in the upper 250 m in the Norske trough, analogous to Figure 25.

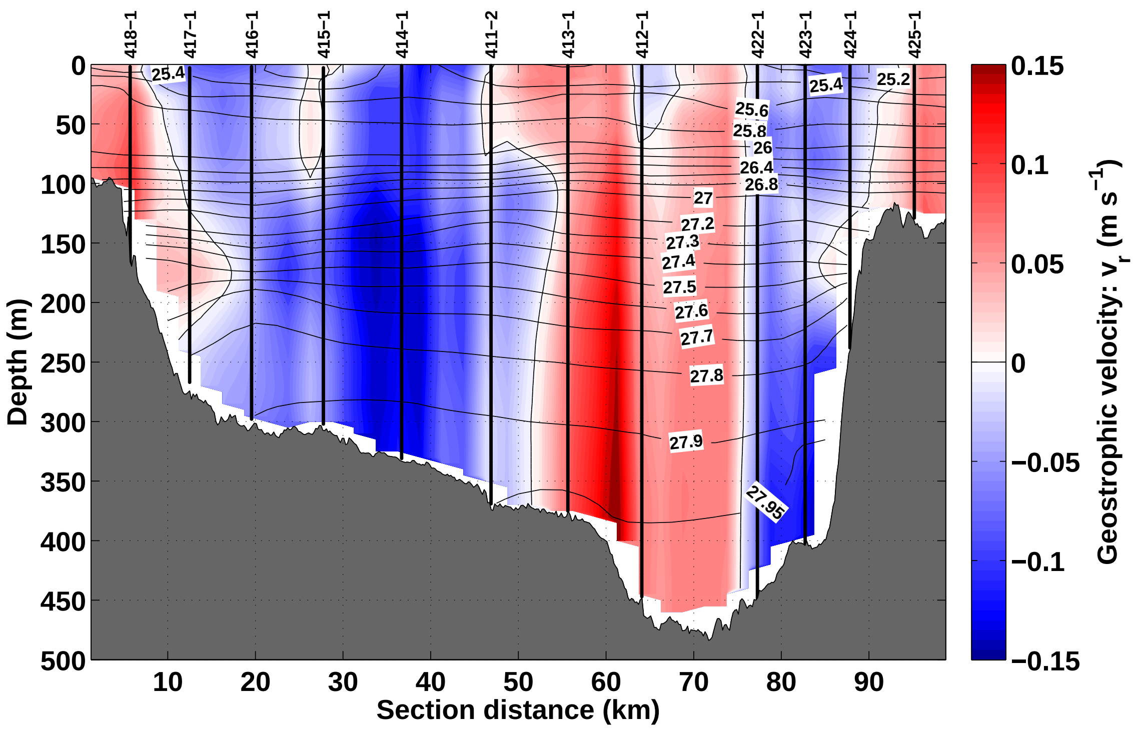

Figure 27: Cross-sectional absolute geostrophic velocity v_r in the Norske trough, based on CTD measurements taken during the *R/V Polarstern* cruise PS85 on 14 June and 15 June 2014. Bold black lines indicate the location of the 12 individual CTD casts and vertical thin black lines represent the zero velocity contour. Horizontal thin black contour lines represent isopycnals. The gridding was done with cubic splines under tension (Smith and Wessel, 1990). The bathymetry shown is based on 200-m averages of the echosounder data collected during all three crossings of the trough.

Table 4: Parameters for the example calculations of the magnetic field for a coiled cable solenoid.

Set-up parameter	**Variable**	**Magnitude**
Relative permeability seawater	$\mu_{r,seawater}$	≈ 1
Number of turns	N	5
Length of solenoid	l	0.02 m
Radius of solenoid	r	0.1 m

Table 5: Typical magnetic field strength B at a point on the longitudinal axis outside a coiled cable solenoid for different distances x_1 and currents I. The magnetic field is also shown for 3 similar solenoids that are aligned in such a way that their magnetic fields add up.

$\boldsymbol{x_1}$	**I**	**B(z)**	**B(z) for 3 aligned solenoids**
0.05 m	0.1 A	519 nT	1557 nT
	1 A	5191 nT	15573 nT
0.1 m	0.1 A	91 nT	274 nT
	1 A	913 nT	2739 nT
0.2 m	0.1 A	13 nT	40 nT
	1 A	134 nT	403 nT

Table 6: Earth's magnetic field components at 77.5° N 15° W on 1 June 2014. Values are based on the International Geomagnetic Reference Field (IGRF) provided on `http://www.ngdc.noaa.gov/geomag-web/\#igrfwmm`.

Field component	**Magnitude**
Total field	54441 nT
Vertical component	53896 nT
East component	-1981 nT
North component	7201 nT
Horizontal intensity	7469 nT